NASA/CR-2005-213911

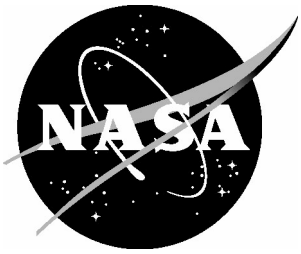

Enhancements of Tow-Steering Design Techniques: Design of Rectangular Panel Under Combined Loads

Brian F. Tatting, and Shahriar Setoodeh
ADOPTECH, Inc., Blacksburg, Virginia

Zafer Gürdal
Virginia Polytechnic Institute and State University, Blacksburg, Virginia

September 2005

The NASA STI Program Office . . . in Profile

Since its founding, NASA has been dedicated to the advancement of aeronautics and space science. The NASA Scientific and Technical Information (STI) Program Office plays a key part in helping NASA maintain this important role.

The NASA STI Program Office is operated by Langley Research Center, the lead center for NASA's scientific and technical information. The NASA STI Program Office provides access to the NASA STI Database, the largest collection of aeronautical and space science STI in the world. The Program Office is also NASA's institutional mechanism for disseminating the results of its research and development activities. These results are published by NASA in the NASA STI Report Series, which includes the following report types:

- TECHNICAL PUBLICATION. Reports of completed research or a major significant phase of research that present the results of NASA programs and include extensive data or theoretical analysis. Includes compilations of significant scientific and technical data and information deemed to be of continuing reference value. NASA counterpart of peer-reviewed formal professional papers, but having less stringent limitations on manuscript length and extent of graphic presentations.

- TECHNICAL MEMORANDUM. Scientific and technical findings that are preliminary or of specialized interest, e.g., quick release reports, working papers, and bibliographies that contain minimal annotation. Does not contain extensive analysis.

- CONTRACTOR REPORT. Scientific and technical findings by NASA-sponsored contractors and grantees.

- CONFERENCE PUBLICATION. Collected papers from scientific and technical conferences, symposia, seminars, or other meetings sponsored or co-sponsored by NASA.

- SPECIAL PUBLICATION. Scientific, technical, or historical information from NASA programs, projects, and missions, often concerned with subjects having substantial public interest.

- TECHNICAL TRANSLATION. English-language translations of foreign scientific and technical material pertinent to NASA's mission.

Specialized services that complement the STI Program Office's diverse offerings include creating custom thesauri, building customized databases, organizing and publishing research results ... even providing videos.

For more information about the NASA STI Program Office, see the following:

- Access the NASA STI Program Home Page at ***http://www.sti.nasa.gov***

- E-mail your question via the Internet to help@sti.nasa.gov

- Fax your question to the NASA STI Help Desk at (301) 621-0134

- Phone the NASA STI Help Desk at (301) 621-0390

- Write to:
  NASA STI Help Desk
  NASA Center for AeroSpace Information
  7121 Standard Drive
  Hanover, MD 21076-1320

NASA/CR-2005-213911

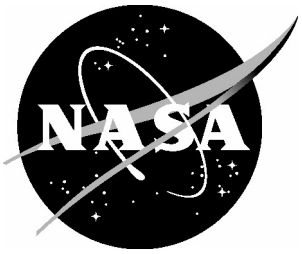

Enhancements of Tow-Steering Design Techniques: Design of Rectangular Panel Under Combined Loads

Brian F. Tatting, and Shahriar Setoodeh
ADOPTECH, Inc., Blacksburg, Virginia

Zafer Gürdal
Virginia Polytechnic Institute and State University, Blacksburg, Virginia

National Aeronautics and
Space Administration

Langley Research Center
Hampton, Virginia 23681-2199

Prepared for Langley Research Center
under Contract NAS1-00135

September 2005

Available from:

NASA Center for AeroSpace Information (CASI)
7121 Standard Drive
Hanover, MD 21076-1320
(301) 621-0390

National Technical Information Service (NTIS)
5285 Port Royal Road
Springfield, VA 22161-2171
(703) 605-6000

Abstract

An extension to existing design tools that utilize tow-steering is presented which is used to investigate the use of elastic tailoring for a flat panel with a central hole under combined loads of compression and shear. The elastic tailoring is characterized by tow-steering within individual lamina as well as a novel approach based on selective reinforcement, which attempts to minimize compliance through the use of Cellular Automata design concepts. The selective reinforcement designs lack any consideration of manufacturing constraints, so a new tow-steered path definition was developed to translate the prototype selective reinforcement designs into manufacturable plies. The minimum weight design of a flat panel under combined loading was based on a model provided by NASA-Langley personnel and analyzed by *STAGS* within the *OLGA* design environment. Baseline designs using traditional straight fiber plies were generated, as well as tow-steered designs which incorporated parallel, tow-drop, and overlap plies within the laminate. These results indicated that the overlap method provided the best improvement with regards to weight and performance as compared to traditional constant stiffness monocoque panels, though the laminates did not measure up to similar designs from the literature using sandwich and isogrid constructions. Further design studies were conducted using various numbers of the selective reinforcement plies at the core and outer surface of the laminate. None of these configurations exhibited notable advantages with regard to weight or buckling performance. This was due to the fact that the minimization of the compliance tended to direct the major stresses toward the center of the panel, which decreased the ability of the structure to withstand loads leading to instability.

1.0 Task Description

The subject of this report concerns the enhancement of proven tow-steering design techniques for laminated composite structures[1-4] through the implementation of novel weight-reduction methods based on a Cellular Automata (*CA*) design methodology. The structural design problem used as a basis of the study involves a flat rectangular panel under combined compression and shear loading, for which a test fixture and alternate designs were previously available.[5] Besides introducing the *CA* design concept, which resembles internal stiffening of the laminate and will be referred to as selective reinforcement, the results will also investigate designs using the standard tow-steering techniques developed in the earlier references. Comparisons of the optimized designs toward existing sandwich and isogrid panel constructions will be used to indicate if manufacture and testing of the tow-steered/selective reinforcement designs is warranted in the future.

2.0 Problem Definition and Model Synthesis

The problem under consideration consists of a flat panel with a 3-inch diameter central hole loaded by combined forces of compression and shear. A complete *STAGS* model detailing the structure under realistic test conditions was supplied to ADOPTECH by NASA-Langley personnel, and subsequently transformed into a slightly simpler model (in terms of edge conditions and additional elements required for accurate modeling) to facilitate the design techniques. This section describes the geometry of the problem and the associated simplifications to the model, while more detail of the model synthesis is supplied in the appendix.

A three-dimensional representation of the finite element model is shown below in Figure 1 (without the central hole for simplicity). The model consists of a test panel (the regular grid in the center region)

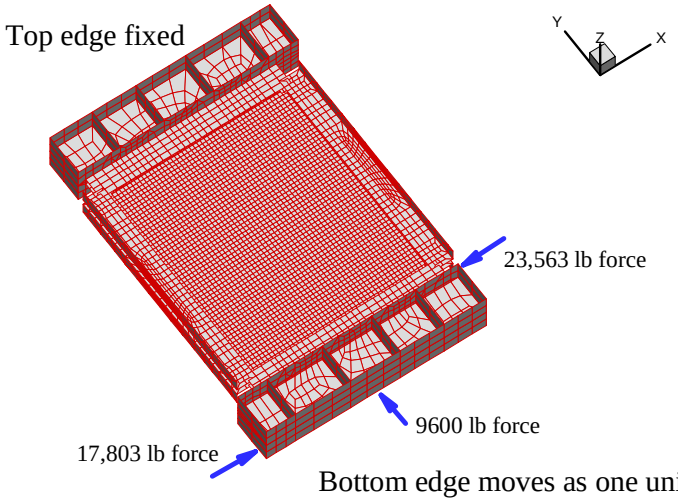

Figure 1: Geometry of Combined Loading Test Fixture and Specimen

attached on each side to a picture-frame-type fixture that is connected by pins, which is attached to appropriate loading frames to achieve the combined loading stress state. During testing, the top edge of the upper frame is held fixed, while the bottom frame undergoes a vertical force from below and a horizontal force through an L-extension of the bottom frame (not shown here). This results in a horizontal force as well as a bending moment, which is represented in the *STAGS* model by the force couple shown.

The test panel area is 24 inches wide and 28 inches high, with a grid size of one-half inch in both directions. The original model is assumed to be composed of aluminum (E = 10.0 Msi, ν = 0.33) with a

thickness of 0.125 inches. One element is removed at each corner of the test coupon to alleviate stress. Tabs are present on all four sides. The top and bottom tabs measure 23 inches wide (due to the 1/2 cut-out in each corner) by 2.94 inches high, while the sides are 27 inches high and 2.25 inches wide. The tabs are constructed with a layer of steel (E = 30.0 Msi, ν = 0.30, 0.19 inches thick) bonded to each side (though the tab material may change for composite materials, we can assume that one will be present and will use the steel tab assumption hereafter). The test panel and tabs are shown in Figure 2 below with the other components removed. The origin of the axes is in the bottom left corner of the test panel. Note that the meshing within the tabbed regions is quite erratic, which is due to the fact that earlier models possessed higher density meshes within the test panel region along with the fact that certain points within the tab had to be defined as nodes. These nodes are denoted by the colored dots in the figure, and represent the points of attachment between the tabbed regions and the fixture. The blue dots represent nodes in the tabs which are defined within the model as having identical displacements (horizontal u, vertical v, and out-of-plane w) as the corresponding point in the frame. The green dots are similarly defined, but are only constrained in the u and w displacement directions (the connections in the side fixtures are slotted to allow vertical movement). The red dots shown here represent the pinned connections between horizontal and vertical components of the fixture, and indicate that the displacements for each connected component are identical at that point (note that no connection to the test panel or tabbed areas exist for these red points, but are shown for completeness).

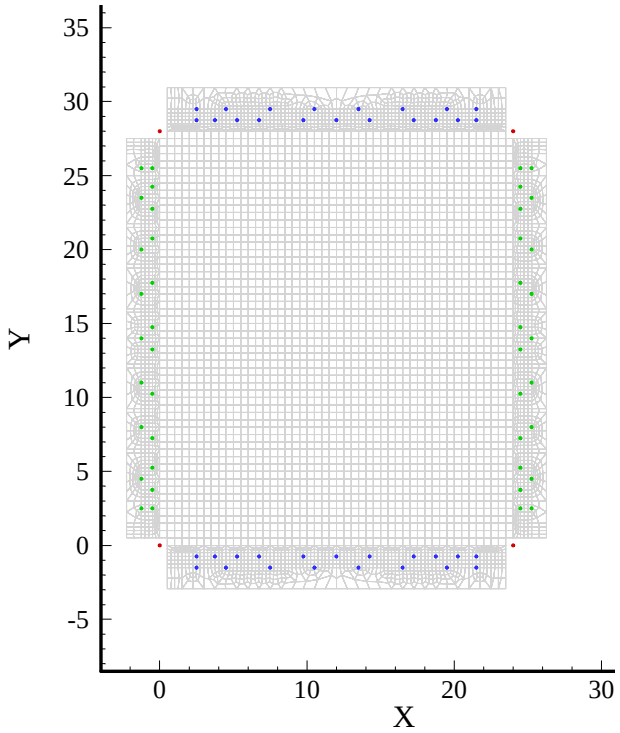

Figure 2: Original Mesh of Laminate and Tabbed Regions (hole not shown)

Several stages of test model simplifications were used to simplify the model for design use. This mostly consisted of replacing the loading frame structure with equivalent boundary conditions and/or shell wall construction definitions so that the physics was still accurately modeled while minimizing the number of elements in the model. Implementation of these changes is catalogued in the appendix, and results in the model shown in Figure 3 for use within the design environment.

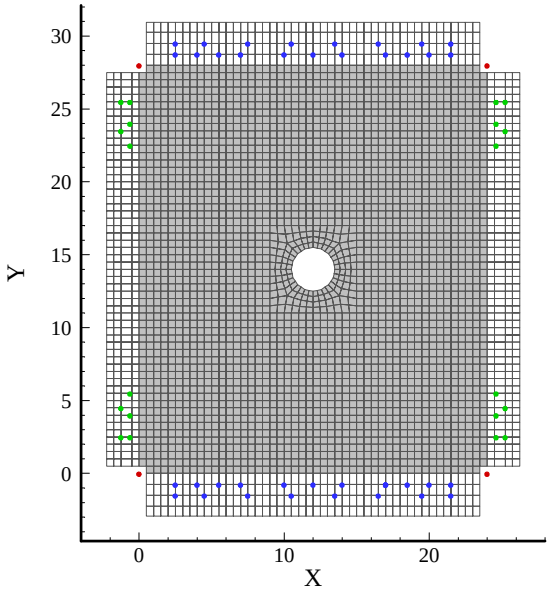

Figure 3: Idealized Mesh of Laminate and Tabbed Regions

STAGS analysis produces the following results for this model. The numbers in parentheses represent the percent change from the original model for the important quantities, with the most relevant quantities being the eigenvalue and computation time:

STAGS results for ideal model:		
u-displacement of top edge (*x*=12, *y*=28)	=	-0.000072
u-displacement of bottom edge (*x*=12, *y*=0)	=	-0.022836
Relative *u*-displacement	**=**	**-0.022764 (2.6%)**
v-displacement of top edge (*x*=12, *y*=28)	=	0.0000302
v-displacement of bottom edge (*x*=12, *y*=0)	=	0.0061293
v-displacement of bottom edge node (*x*=21.5, *y*=0)	=	0.0060623
Relative rotation of bottom edge	=	-7.053×10^{-6} radians
Relative *v*-displacement	**=**	**0.0060991 (7.5%)**
Eigenvalue of linear buckling solution	**=**	**0.71818 (2.0%)**
Computation time (sec)	**=**	**49.8 (-70.8%)**

These results satisfy the goals of the model synthesis, providing a suitably accurate model with a significant decrease in computation time. More detail concerning the attributes of this model and the alterations from the original configuration (Figure 2) are provided in the appendix.

3.0 Ply Design using Cellular Automata Solutions

For the Cellular Automata (*CA*) design study, an equivalent model was constructed using the same dimensions and boundary conditions as the *STAGS* model (along with a 3-inch diameter central hole). Additionally, the mesh spacing within the tabbed regions was re-ordered with ½-inch square elements to facilitate definition within the Cellular Automata design technique. The *CA* design technique used the equivalent model to estimate the stiffness response of the structure subjected to axial compression and shear (the shear being applied as two different load cases in opposite directions). Topology methods were then used to reduce the weight of the structure (which was assumed to be constructed of a single ply) to a

specified volume fraction while minimizing the compliance of the structure. Note that no buckling estimations were used here; the designs were motivated by the topology design based on minimum compliance design. Further details of the topology design problem using this approach can be found in references 6 and 7.

The problem of minimum compliance design was initially solved using fiber angles as continuous spatial design variables. Numerical experiments showed that substantial stiffness improvements can be gained only by re-orientation of the orthotropic material in an optimal manner. However, this formulation requires repeated transformation of the material properties using the classical trigonometric transformations. These transformations are not only expensive in terms of the computational costs, but also can cause convergence problems. A more rigorous formulation for the same compliance design problem is to use the lamination parameters as design variables instead of the fiber angles. The in-plane behavior of balanced symmetric laminates can be fully modeled using only two lamination parameters regardless of the actual number of layers. Moreover, the laminate extensional stiffness matrix is linear in terms of the lamination parameters. It can also be shown that compliance is convex in the lamination parameters space. These characteristics are very beneficial in the optimal design of laminated composites in the sense that they substantially improve the computational efficiency as well as the accuracy. However, transformation of these lamination parameter designs into manufacturable tow-steered plies is an intricate process that does not always lead to a viable solution. Furthermore, the results using the lamination parameters did not produce designs with lower compliance as compared to the method based on fiber orientation angles. Therefore, the design study implemented the fiber angle methodology and was limited to one-ply configurations, which could then later be transformed into viable candidates for stacking sequence design.

During the design study, the *CA* design methodology was updated in several respects to facilitate better design results. As mentioned, one such improvement was to include multiple load cases (both positive and negative shear) within the analysis portion. This improvement also contained procedures to implement the combined in-plane bending/compression of the panel through a linear combination of displacement loading, which was required to attain the correct level of accuracy as compared to the original *STAGS* model. Options considering the symmetry of the design were also considered, so that the user could decide if symmetry was required in the vertical or horizontal directions. Local balancing could be stipulated using the lamination parameters formulation, though the results are not shown here due to the inferiority of the designs using this constraint.

3.1 Candidate Designs for Selective Reinforcement

Using the available options within the *CA* design software, the following results were obtained for the problem under study. Note that the figures are for one ply only, and manufacturability has not been taken into consideration yet. The colors of the elements represent the fiber orientation angle, which is further displayed by the directional lines at the center of each element. The compliances and volume fractions for each design is given within the table. Designs in the first column were constrained to be symmetric in both the x- and y-directions, while for the second column the y-symmetry condition was removed.

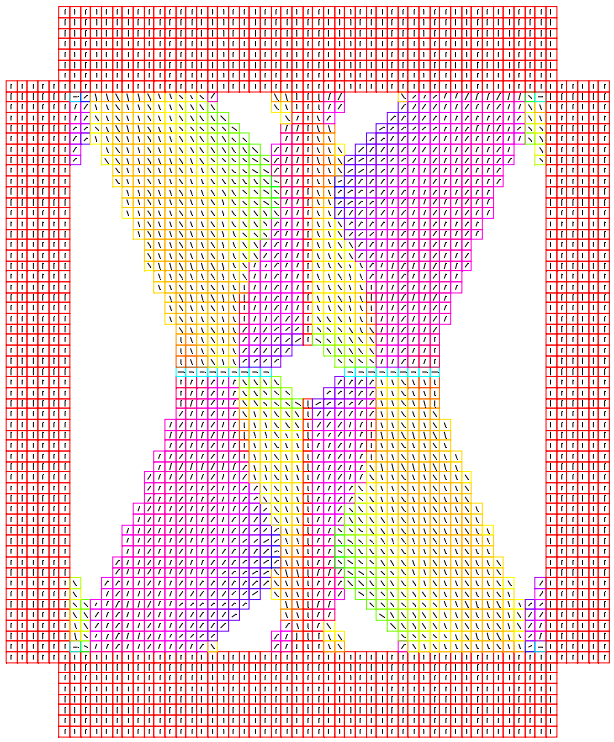

Compliance = 303.21 N·m

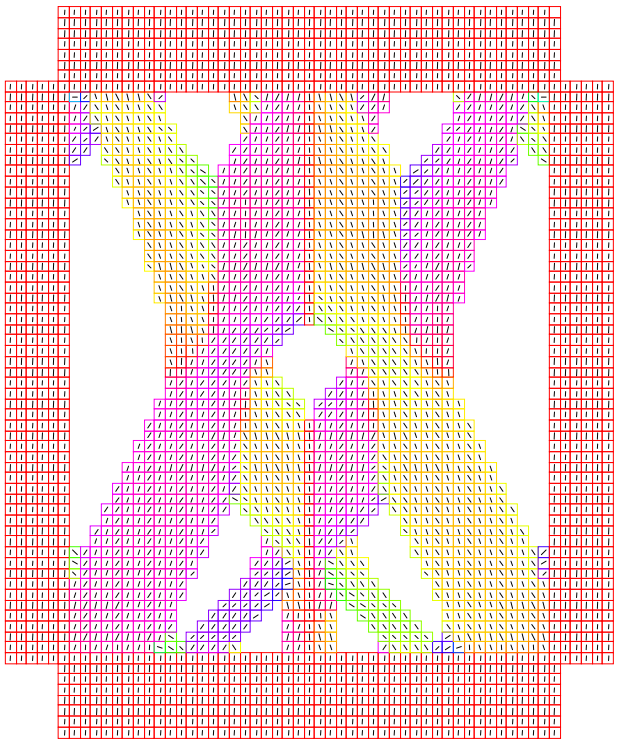

Compliance = 331.43 N·m

70% Volume Fraction

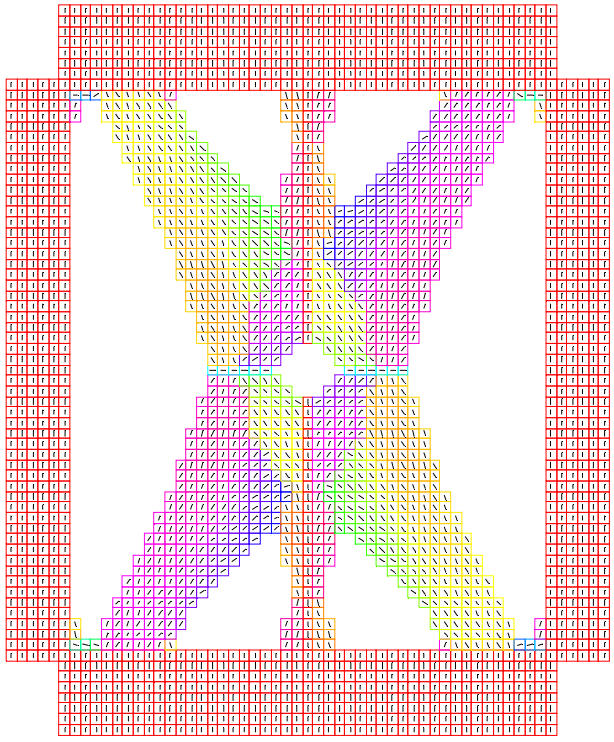

Compliance = 441.52 N·m

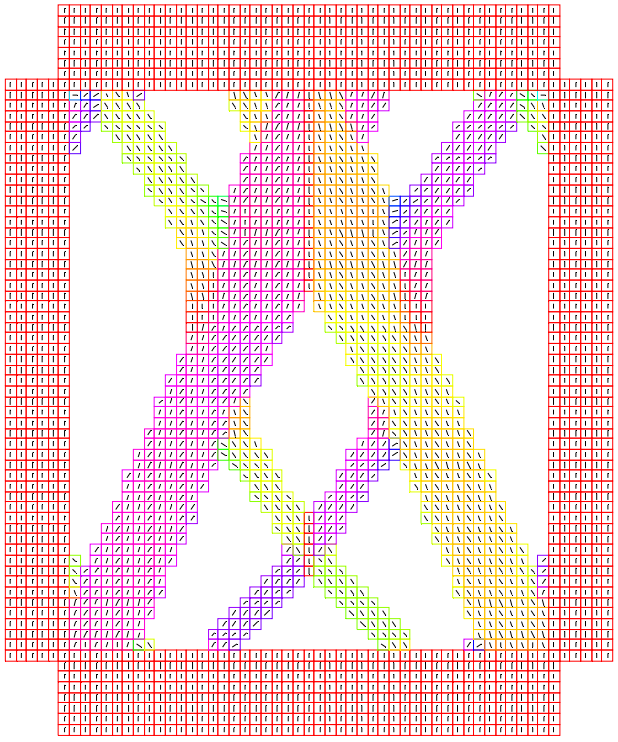

Compliance = 456.54 N·m

50% Volume Fraction

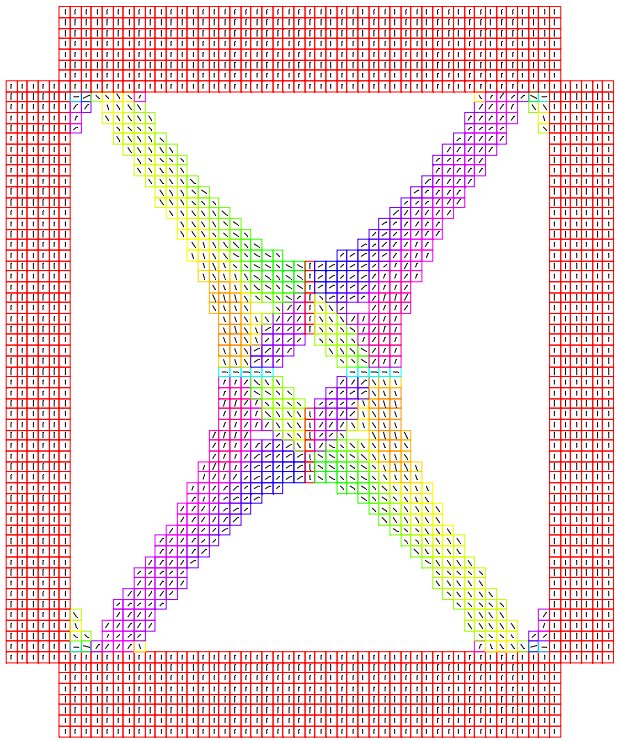	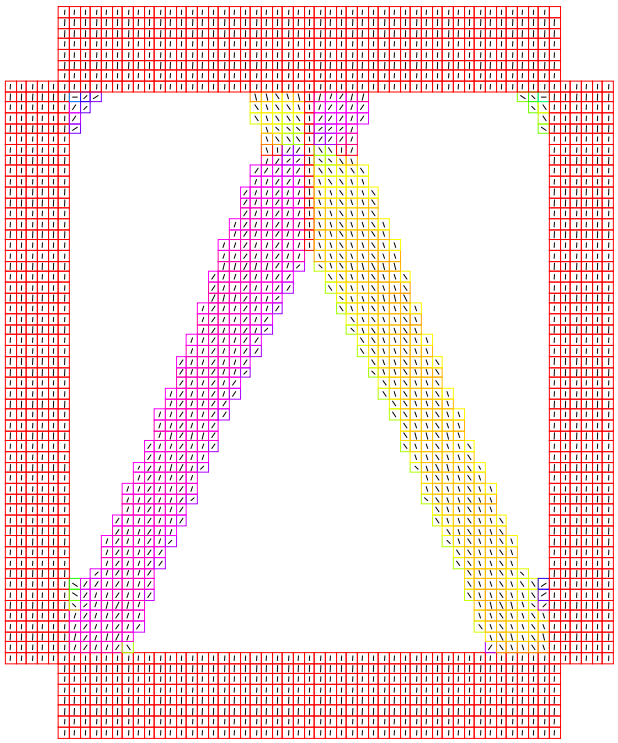
Compliance = 698.42 N·m	*Compliance = 612.92* N·m
30% Volume Fraction	
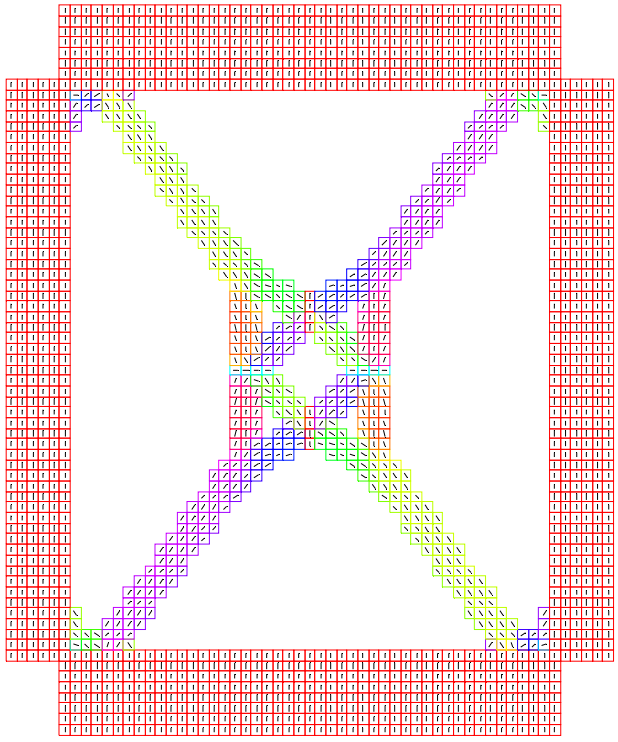	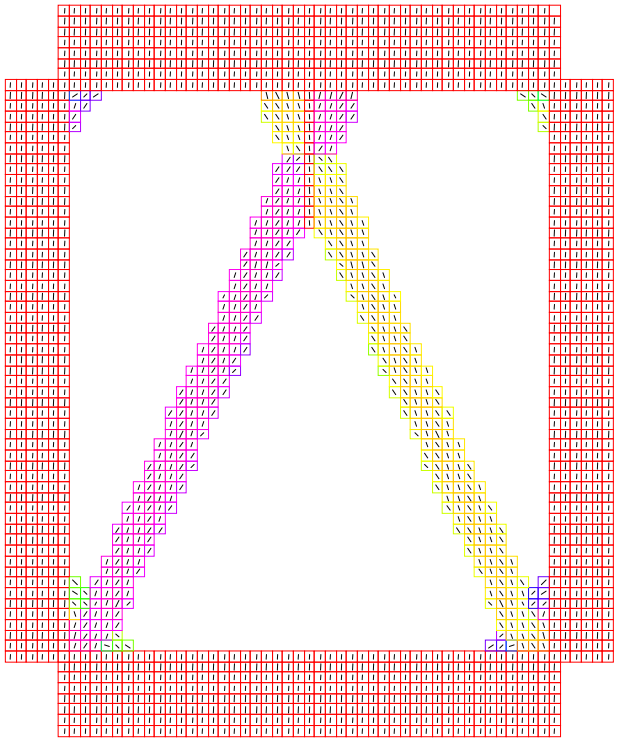
Compliance = 985.73 N·m	*Compliance = 766.66* N·m
20% Volume Fraction	

3.2 Manufacturing Concerns and Tow-Steering Definitions

As opposed to typical tow-steered design techniques used by ADOPTECH's *OLGA* software, the *CA* design algorithm does not take manufacturability into account during the design process. This is quite evident in the results of the previous table, which indicate idealized ply orientation angles that would be difficult, if not impossible, to construct using real-world fabrication techniques. Therefore, the candidate designs were inspected by hand to determine which candidates were best suited for slight alterations that would enable manufacture. This task was completed prior to the next design step, so that only manufacturable designs are considered in the final design process.

From the results of the previous table, it was decided that the designs with the higher volume fraction (70% and 50%) were too irregular for a suitable transformation to a manufacturable design. This was also true for the full coverage design (not shown), which resulted in patches of differing fiber orientation angle throughout the ply. Though some improvements with regard to manufacturability can be specified within the *CA* algorithm (such as limiting the orientation angles to discrete values), the resulting designs still contain these smaller patches which require significant tow-dropping within each ply. When implemented with an advanced tow-placement machine, the minimum cut length parameter associated with the cut/restart capability of the manufacturing process becomes a critical constraint which cannot always be satisfied by the idealized configurations. The minimum turning radius constraint also needs to be considered when variations in fiber orientation angle along a path were desired. Therefore, attention was focused on the remaining designs (30% and 20% volume fractions), which had definitive paths that were more conducive to tow-placement methods.

3.2.1 Tow-steered definition based on Piecewise Arc formulation

With regard to the 30% and 20% volume fraction *CA* designs, it is evident that the plies could be approximated by tow-steered paths of varying widths. Therefore, a new tow-steering path definition was formulated to reflect the variations that were required from the *CA* results and inserted into the catalog of tow-steering definitions already developed by ADOPTECH.[1,3] The new path definition is dubbed "Piecewise Arc", and is at the same level within the hierarchy as the "Linear Angle" and "Circular Arc" definitions referred to in the references.

It is evident that the main mechanism for the 20% and 30% volume fraction designs is paths that tend to surround the central hole. Upon further inspection, various curvilinear paths could be constructed by hand to adequately simulate the desired ply coverage. However, it was easily seen that most of the constructions violated the curvature constraint for the tow-placement machine (here assumed to be a turning radius of 25 inches). Therefore, two options existed to model the given designs: to use multiple straight fiber paths with significant tow-dropping; or to use curvilinear plies with maximum allowable curvature that would approximate the desired configuration. The choice of curvilinear paths was motivated by the fact that (1) the straight fiber paths for the given designs might also have problems with the minimum cut length parameter; (2) the amount of tow-dropping required would lead to a slow manufacturing process for the ply; and (3) paths that run from one boundary of the structure to another constitute a more reliable structural configuration.

Therefore, suitable curvilinear paths were considered for the modeling of these designs. Based upon earlier work, simple constructions based on constant curvature arcs were introduced. Like earlier definitions, these constructions used a handful of parameters to provide enable easy definition while still remaining general enough to produce a large variety of designs. The basic path, shown schematically in Figure 4 and hereby referred to as the *piecewise arc* reference path, assumes that a straight line is interrupted by four arcs of constant curvature that are intended to curve around the region of interest. The user-defined parameters are the characteristic distance d, which must be positive and represents the length of the opening ($d = d_0 + d_1$ in the figure), and two angles which represent spans of the arc. These angles must be between -90 and 90 degrees. The path consists of a straight line merging into a constant radius

arc (as an option, the radius r of the arcs may be input instead of d), which opens concave upward or downward depending on the sign of T_0. After the prescribed arc is completed, the path returns to the horizontal through an identical arc. At that point, another arc is begun, this time turning through T_1 degrees and back again until the horizontal is again reached. The line then continues ad infinitum.

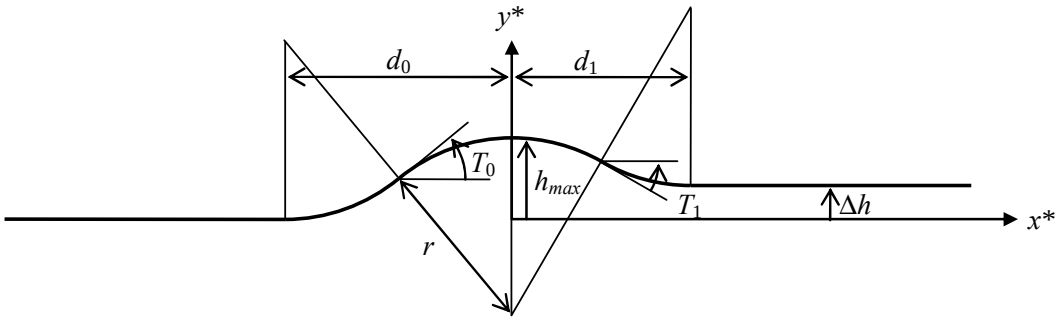

Figure 4: Piecewise Arc Reference Path

The relevant equations defining the radius of the arcs and the width of the opening are given as:

$$\begin{aligned} &d = d_0 + d_1 \quad d_0 = 2r\sin|T_0| \quad d_1 = 2r\sin|T_1| \\ &r = \frac{d}{2\left(\sin|T_0| + \sin|T_1|\right)} \\ &h_{\max} = 2r\left(1-\cos T_0\right)\mathrm{sgn}\left(T_0\right) \qquad \Delta h = 2r\left(\cos T_1 - \cos T_0\right)\mathrm{sgn}\left(T_0\right) \end{aligned} \tag{1}$$

Note that for $T_1 = -T_0$ (the most usual configuration), $r = d/4\sin|T_0|$ and $\Delta h = 0$. Perfectly straight lines are stipulated with zero values for T_0 and T_1.

To construct a complete ply course, a head width *hw* is supplied and parallel curves at a distance ±*hw*/2 are created that represent the course edges. Additionally, a path mirrored about the *x**-axis is constructed to complete the pair of paths (using negative values for the angle parameters). The vertical location of the mirrored path is determined by the value of the *overlap* parameter, so that the paths can be collinear or possess a gap between the horizontal lines. Where overlapping occurs, the choice of tow-dropping or thickness variation can be set by the user, and the locations of tow-drops are determined to maximize the cut length along a tow. A sample of a ply using these techniques combining the two mirrored paths is shown in Figure 5.

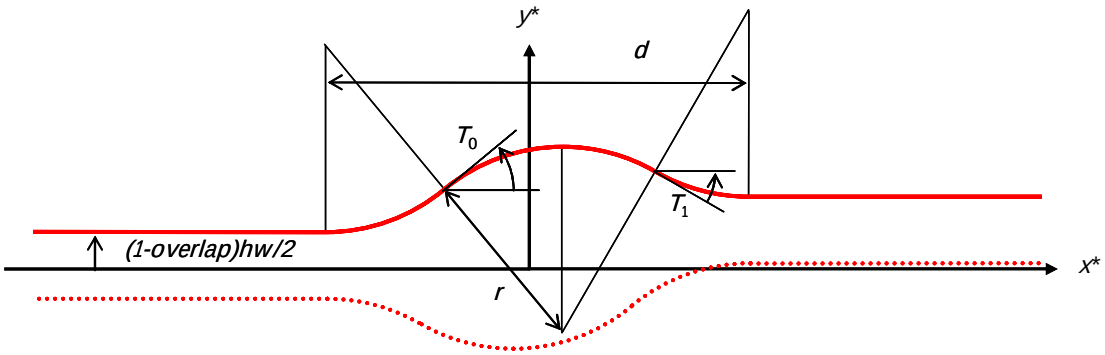

Figure 5: Mirrored Paths using the Piecewise Arc Reference Path

Lastly, the set of two courses can be positioned and rotated within the structure through the use of a global translation and rotation of the x^*y^*-axis, as defined for other path variations in earlier work (parameters $\{x_0, y_0\}$ and ϕ). Algorithms exists that can extract the relevant fiber orientation information for a given point within the surface of the laminate. Balanced plies can also be included in the construction of the laminate, which automatically provide some symmetry and ensure that continuous paths are constructed equally in both directions. Some examples of this tow-steered ply definition are shown in Figure 6, where the origin of the stiffness variation is assumed to be in the center of the panel.

Symmetric ply example

Tow Drop method
Origin = {0, 0}
$\phi = 30°$
$d = 25"$
$T_0 = 15°$
$T_1 = -15°$
overlap = 1
hw = 2"

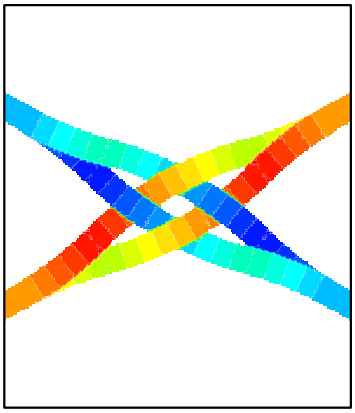

Unsymmetric ply example

Tow Drop method
Origin = {0, -3.35"}
$\phi = 0°$
$d = 25"$
$T_0 = 15°$
$T_1 = 0°$
overlap = -2
hw = 2"

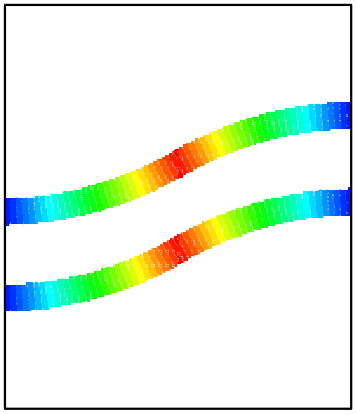

Interlocking straight path example

Overlap method
Origin = {5", 2"}
$\phi = 25°$
$T_0 = T_1 = 0°$
overlap = -2
hw = 2"

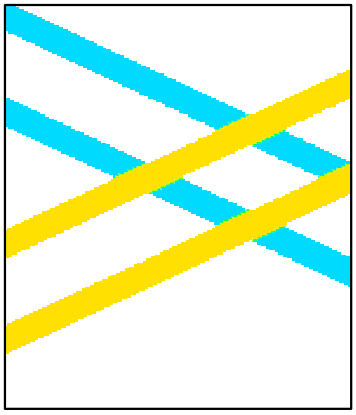

Figure 6: Examples of Piecewise Arc Construction Method

3.2.2 Tow-steered plies from candidate CA designs

With the *piecewise arc* formulation in hand, parameters are chosen to best resemble the candidate designs found from the *CA* design study in Section 3.1. For these definitions, a minimum cut length of 5 inches and a minimum turning radius of 25 inches is assumed according to specifications from a typical tow-placement machine. Vertically symmetric plies will also be formulated, where needed, to fully explore the possibilities for the selective reinforcement plies.

Ply Set #1: 30% Straight

(a) Overlap method
Origin = {0, 11"}
$\phi = 67.5°$
$T_0 = T_1 = 0°$
overlap = 1
hw = 3"
(see Figure 7)

(b) Identical except for
Origin = {0, 0}
overlap = -1.81
(vertically symmetric, similar to Figure 8)

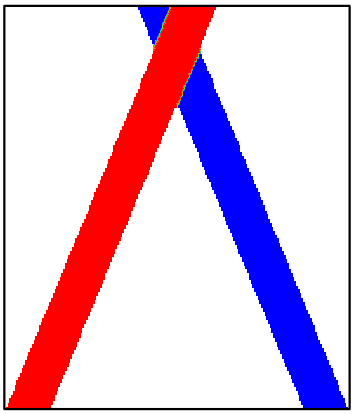

Figure 7: Ply 1a

Ply Set #2: 20% Straight

(a) Overlap method
Origin = {0, 11"}
$\phi = 66°$
$T_0 = T_1 = 0°$
overlap = 1
hw = 2.25"
(similar to Figure 7)

(b) Identical except for
Origin = {0, 0}
overlap = -2.98
(see Figure 8)

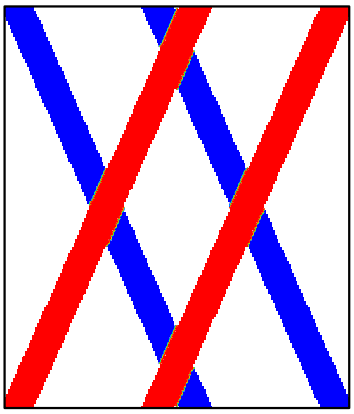

Figure 8: Ply 2b

Ply Set #3: 30% Curvilinear

(a) Overlap method
Origin = {0, 0}
$\phi = 54.375°$
d = 25.88"
$T_0 = 15°$
$T_1 = -15°$
overlap = 1
hw = 1.5"
(see Figure 9)

(b) Identical except uses Tow Drop method
(similar to Figure 10)

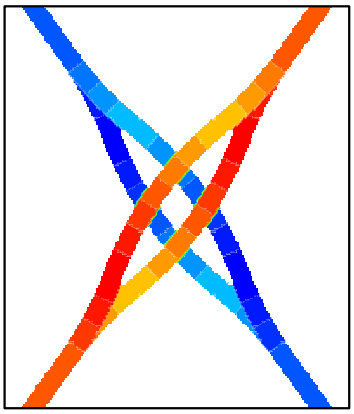

Figure 9: Ply 3a

Ply Set #4: 20% Curvilinear

(a) Overlap method
Origin = {0, 0}
ϕ = 54.375°
d = 25.88"
T_0 = 15°
T_1 = -15°
overlap = 1
hw = 1"
(similar to Figure 9)

(b) Identical except uses Tow Drop method
(see Figure 10)

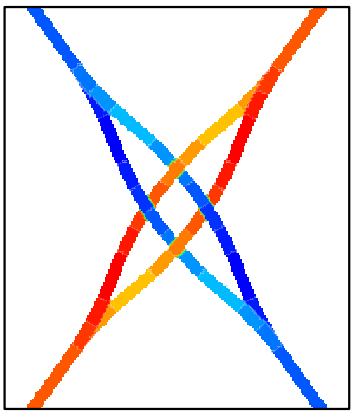

Figure 10: Ply 4b

4.0 Design Study Formulation and Results

The goal of the design study is to ascertain the weight savings potential of the tow-steering and selective reinforcement design schemes for the combined loading configuration. Due to the limitations of the *STAGS*[8] finite element code (version 4), material failure constraints are not able to assessed when using the tow-steered ply definitions (through the *WALL* user-written subroutine that defines the stacking sequence). Therefore the design study will consider only the "linear' buckling loads as the limiting load constraints. Though significant post-buckling deformation will occur before ultimate failure for this structure, the computation time associated with the complex nonlinear solutions are not warranted in this exploratory design phase.

Published literature[5] associated with the test fixture used here has demonstrated that sandwich panels can withstand the designated loads while achieving weight densities as low as 0.49 lb/ft^2. Therefore the ideal goal of the design study is to find non-sandwich laminates that utilize tow-steering and remain competitive with these weight densities. Unfortunately, sandwich panels possess a tremendous advantage as compared to monolithic laminates when only buckling is considered (due to the high bending stiffness produced by the relatively thick sandwich core), so that reaching this goal is not realistic. Instead, it was decided to find the best configurations using these novel design techniques that do not use sandwich construction and compare the results to traditional straight fiber laminates. Future work could later integrate the tow-steering concepts within the face sheet if sandwich construction is warranted.

4.1 Design Study Roadmap

The approach used to investigate the design space afforded by the tow-steering and selective reinforcement options is built upon improving from baseline constant stiffness and unstiffened designs. The laminate will assumed to be constructed of multiple layers of IM7/8552 composite, with a ply thickness of 0.004 inches and a density of 98.5 lb/ft^3 (0.057 lb/in^3). The laminate is assumed to be symmetric about the mid-plane, and laminate balance is achieved automatically by the laminate design software by using balanced two-ply stacks for all ply angle variables. The selective reinforcement plies can be situated either on the interior or the exterior of the laminate, but their number and configuration do not vary within the design process. That is, the type and number of selective reinforcement layers are chosen and then the rest of the laminate (using either traditional straight plies or tow-steered configurations) is designed around the base laminate. Within the *OLGA* design process, weight reduction is performed using a Genetic Algorithm developed specifically for stacking sequence optimization, which takes into account balancing and symmetry and strives to find the laminate with the smallest number of layers that satisfy the buckling load constraint. Ply angle variables are generally in increments of 15°,

though for tow-steered plies some candidate plies are not considered due to violation of the manufacturing constraints (also calculated automatically by the design software). Results will be reported in terms of the stacking sequence for each laminate, the weight density for the structure, and the load factor for instability (a value less than one indicates that buckling is achieved, while larger values indicate that the structure buckles at a higher level than the design load). Design runs on a Windows-based computer require around six hours to complete, therefore some thought is required so as to minimize the number of runs while adequately investigating the design space.

The "roadmap" to find the best design follows the diagram shown in Figure 11. First, a baseline design using only straight fiber plies within the laminate is determined. Secondly, tow-steered plies are introduced within the unstiffened laminate, using previous construction techniques and various stiffness variation directions. These results should indicate the tow-steered construction techniques and preferred directions that show the most promise. The next step investigates the influence of the eight selective

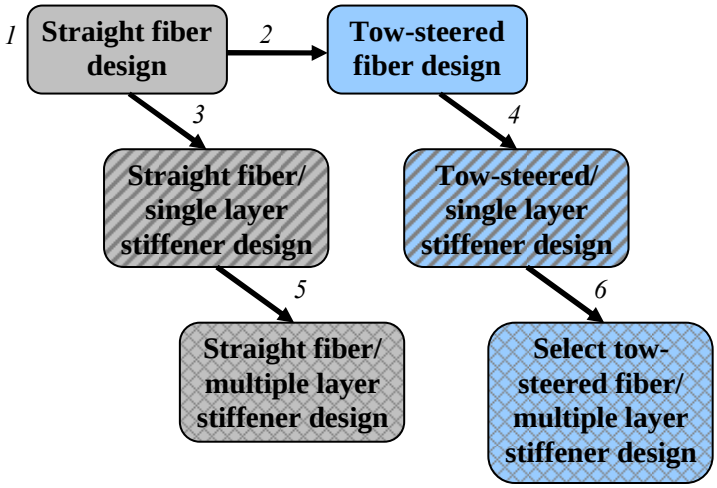

Figure 11: Roadmap for Design Study Organization

reinforcement configurations (ply sets 1a-4b) inserted into the interior of the laminate and surrounded by constant stiffness plies. Note that locating the pseudo-stiffeners at the interior of the laminate is preferred to ensure a more robust external surface for the manufactured laminate. The selective reinforcement plies that provide the best increase in performance will then be used in conjunction with the tow-steered plies as the external laminate, to explore non-intuitive regions of the design space. At this point, there should be strong indications as to the best stiffener arrangement and tow-steered construction technique. The last step will be to determine the effect of increasing the number of plies within the internal stiffener and to investigate the possibility of locating the selective reinforcement plies on the outside of the laminate (even though this construction technique may lead to an inferior laminate construction). This strategy should provide a useful reflection of the available design space and point to the potential sources of performance gains.

4.2 Results and Discussion

Baseline Case:

The baseline design case using straight fiber plies only resulted in a 36-ply laminate with stacking sequence $[\pm 45/\pm 30_3/\pm 15_5]_s$, possessing a weight density of 1.182 lb/ft^2 with a buckling load factor of 1.104. As hinted earlier, this weight density is not comparable to the lightest weight sandwich panel from the literature, but serves as the base comparison for our novel laminate design techniques.

Tow-steered designs with no selective reinforcement:

Six distinct tow-steered construction techniques were used for this portion of the study. Three different ply construction methods are used, namely Parallel, Tow Drop, and Overlap, with the major direction of variation being either horizontal or vertical for each case with the variation axis located at the center of the hole. The Circular Arc formulation (see reference 3) was used as the reference path. The characteristic distance *d* that is used to define the tow-steering variation was chosen as half of the width or height according to the major variation direction. Using the standard minimum turning radius of 25 inches and 15° angle increments generated the following manufacturable designs for each case (as well as the constant stiffness plies for all cases, which are the only plies allowed on the laminate outer surface):

Parallel method

Horizontal variation: 0<0|15>, 0<0|30>, 0<15|0>, 0<15|30>, 0<15|45>, 0<30|15>, 0<30|45>, 0<30|60>, 0<45|15>, 0<45|30>, 0<45|60>, 0<45|75>, 0<60|30>, 0<60|45>, 0<60|75>, 0<75|45>, 0<75|60>

Vertical variation: 90<-75|-60>, 90<-75|-45>, 90<-75|-30>, 90<-60|-75>, 90<-60|-45>, 90<-60|-30>, 90<-45|-75>, 90<-45|-60>, 90<-45|-30>, 90<-45|-15>, 90<-30|-75>, 90<-30|-60>, 90<-30|-45>, 90<-30|-15>, 90<-30|0>, 90<-15|-45>, 90<-15|-30>, 90<-15|0>, 90<-15|15>, 90<0|-30>, 90<0|-15>

Tow Drop and Overlap methods

Horizontal variation: 0<0|15>, 0<0|30>, 0<15|0>, 0<15|30>, 0<15|45>, 0<15|-15>, 0<30|0>, 0<30|15>, 0<30|45>, 0<30|60>, 0<30|75>, 0<45|15>, 0<45|30>, 0<45|60>, 0<45|75>, 0<60|30>, 0<60|45>, 0<60|75>, 0<75|30>, 0<75|45>, 0<75|60>

Vertical variation: 90<-75|-60>, 90<-75|-45>, 90<-75|-30>, 90<-60|-75>, 90<-60|-45>, 90<-60|-30>, 90<-60|-15>, 90<-45|-75>, 90<-45|-60>, 90<-45|-30>, 90<-45|-15>, 90<-30|-75>, 90<-30|-60>, 90<-30|-45>, 90<-30|-15>, 90<-30|0>, 90<-15|-60>, 90<-15|-45>, 90<-15|-30>, 75, 90<-15|0>, 90<-15|15>, 90<0|-30>, 90<0|-15>

The associated weight densities and load factors for the six different tow-steered construction techniques are displayed in Figure 12. Note how the weight densities are the same for most of the construction

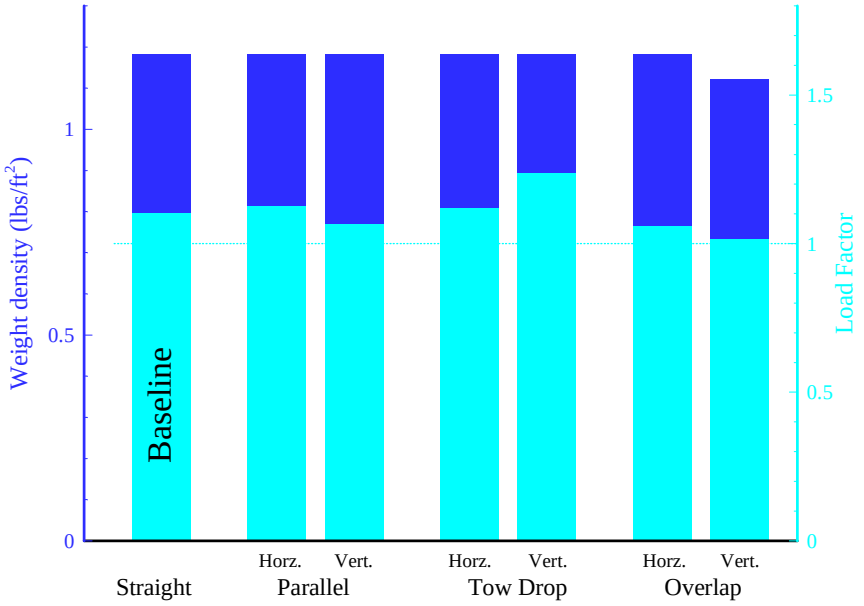

Figure 12: Design Results for Tow-Steered Plies with no Selective Reinforcement

methods, which indicates that the same number of constant thickness plies are used for each design. For the overlap method, the horizontal variation actually converges to a constant stiffness design, while the vertical variation has only 32 plies as well as added weight due to the extra thickness within the overlap regions. The other significant data from the figure concerns the load factor as compared to the baseline design. For the Parallel method with a horizontal stiffness variation (stacking sequence $[\pm 30/0\pm<45|15>_3/0\pm<15|0>/0\pm<45|15>/0\pm<0|30>/0\pm<30|15>/0\pm<0|30>]_s$) and the Tow Drop method with a vertical stiffness variation ($[\pm 30/90\pm<-75|-30>_2/90\pm<-75|-45>_2/\pm 15/90\pm<-75|-60>_3]_s$) the buckling loads are significantly higher than the baseline case, indicating better performance using these configurations. Similarly, though the Overlap method with a vertical stiffness variation has a lower load factor, the fact that the laminate is lighter in weight while still satisfying the constraints indicate the worthiness of the design. The layup for the best Overlap method design is $[\pm 45/90\pm<-60|-30>/\pm 30_2/0_4/90\pm<-75|-60>/0_2]_s$.

Straight fiber designs with single pair of selective reinforcement plies (interior of laminate)

The first test of the selective reinforcement plies uses a single pair (due to symmetry) of stiffeners at the mid-plane of the laminate. Each tow course has a thickness of 0.004 inches, though there do exist local thickness build-ups within overlaps of the courses (for all selective reinforcement plies except 3a and 4a since they utilize tow drops). The rest of the laminate is designed using the standard constant stiffness two-ply stacks in 15° angle increments. The results are shown in Figure 13, and indicate that the selective

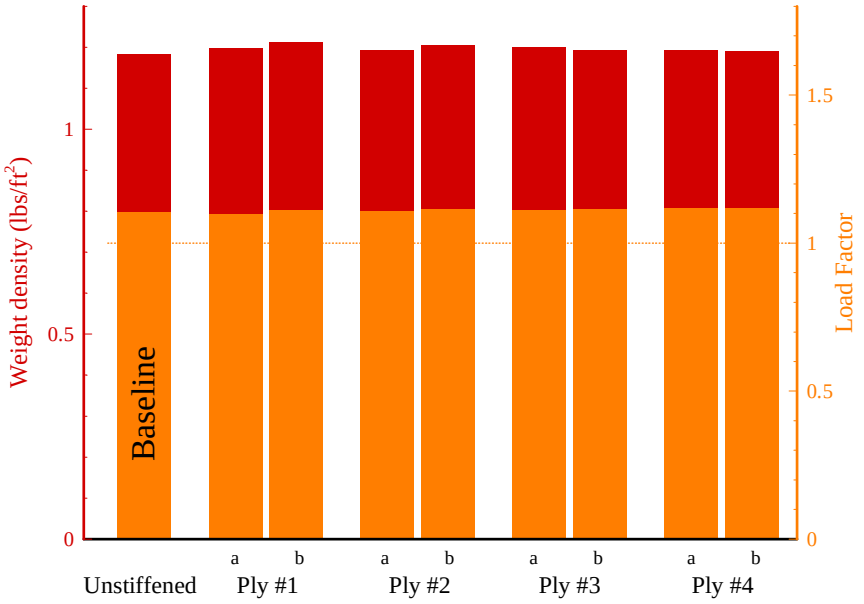

Figure 13: Design Results for Straight Fiber Laminate with Single Pair of Selective Reinforcement Plies (at Interior of Laminate)

reinforcement plies (using a single pair at the interior of the laminate) offer no noticeable improvement over the baseline case. In fact, the introduction of the stiffening regions tends to degrade the performance of the structure, since the load factors are not improved while the weights are slightly increased.

Tow-steered designs with single pair of selective reinforcement plies (interior of laminate)

Similar results to those in Figure 12 can be generated for each of the tow-steered ply construction techniques using a different selective reinforcement scheme. Relevant results for cases 1a, 3b, and 4b are shown in Figure 14-Figure 16, respectively. For all three cases, the stiffness variation that shows the most promise corresponds to the Overlap method with a vertical stiffness variation, while the Parallel/horizontal and Tow Drop/vertical variations exhibit slight increases in the buckling load factor.

However, for the most part weight improvement for all those except the Overlap/vertical variation does not exist.

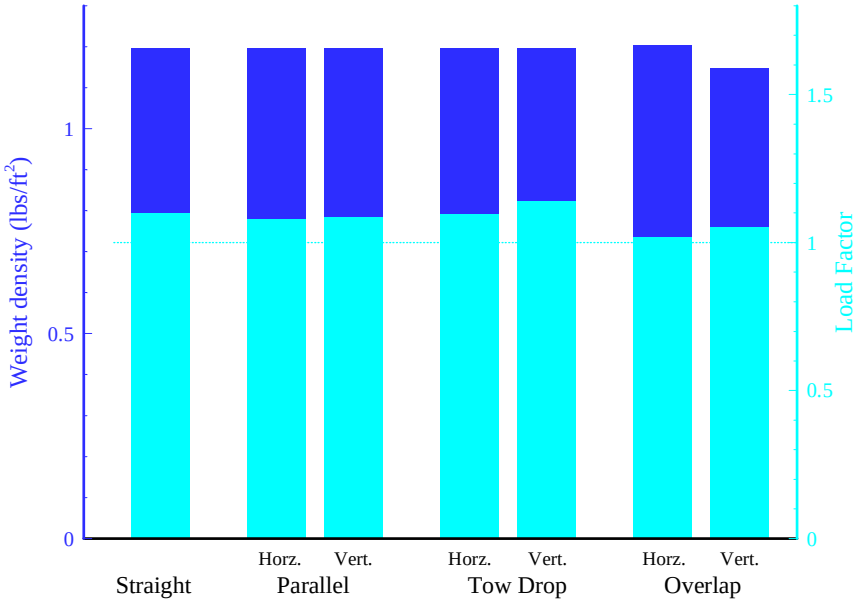

Figure 14: Design Results for Tow-Steered Laminates with Single Pair of 1a Selective Reinforcement Plies (at Interior of Laminate)

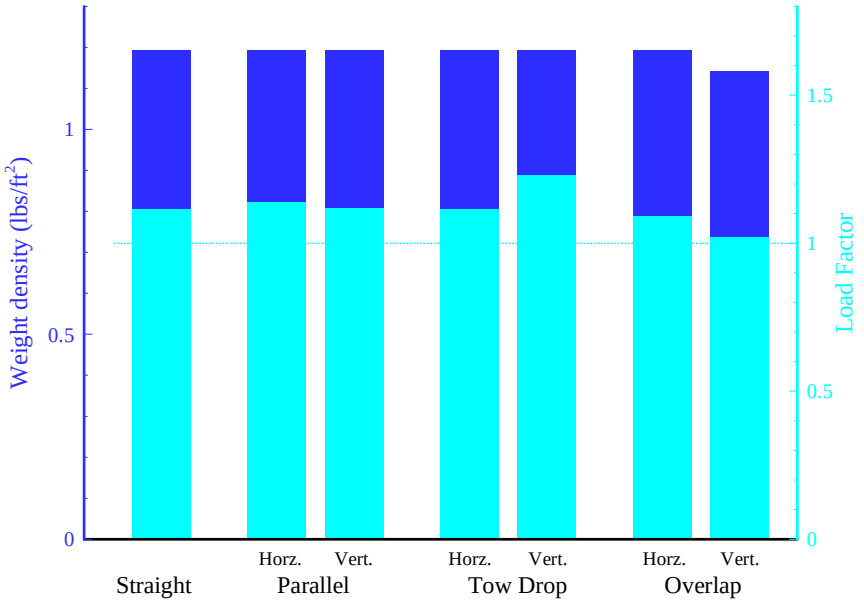

Figure 15: Design Results for Tow-Steered Laminates with Single Pair of 3b Selective Reinforcement Plies (at Interior of Laminate)

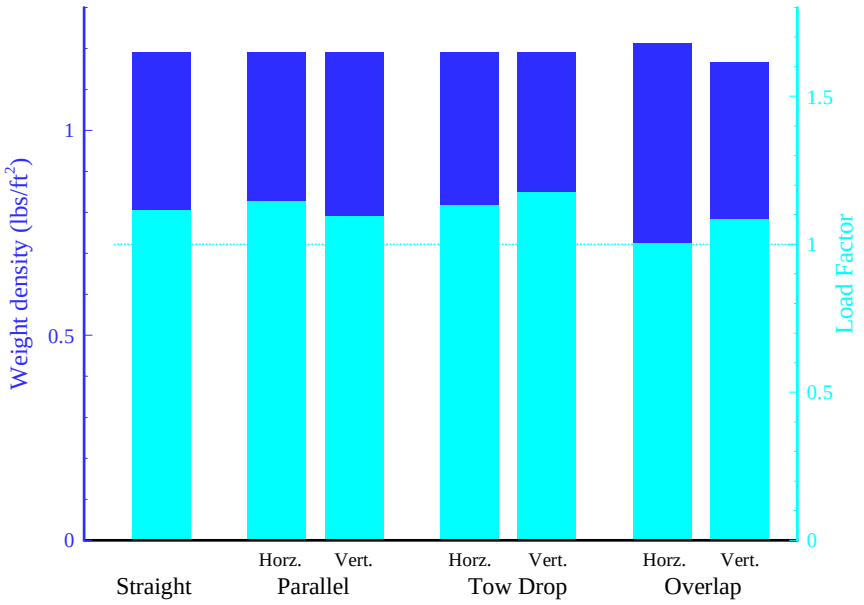

Figure 16: Design Design Results for Tow-Steered Laminates with Single Pair of 4b Selective Reinforcement Plies (at Interior of Laminate)

The results can also be viewed by choosing the best tow-steered construction technique and examining the effect of the selective reinforcement plies. This is displayed in Figure 17 below for the Overlap construction technique using a vertical variation of the stiffness.

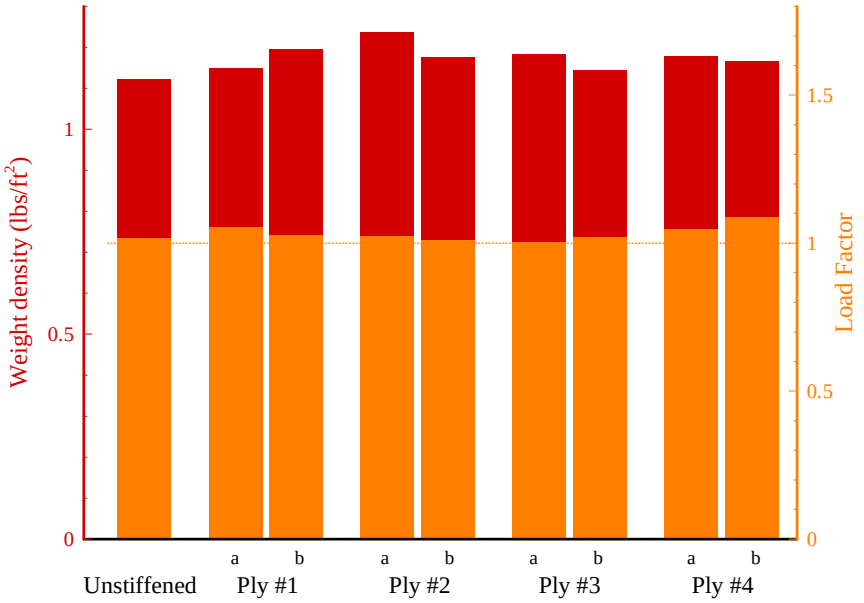

Figure 17: Design Results for Overlap/Vertical Variation Laminate with Single Pair of Selective Reinforcement Plies (at Interior of Laminate)

Note how this compares to Figure 13. Now the versatile overlap method generates noticeable differences between the different selective reinforcement plies. However, it should be noted that the best design in

this group is for the unstiffened laminate, thereby indicating that the presence of the stiffening components still does not contribute to the performance of the structure.

Designs with multiple pairs of selective reinforcement plies

The results of the two previous sub-sections only used a single pair of selective reinforcement plies within the laminate. Design runs were also conducted to investigate the effect of increasing the number of stiffening layers for each configuration. Results for the straight fiber laminate designs using the 4b selective reinforcement case are shown in Figure 18 (other stiffening arrangements exhibited similar results). Note how both the weight density and load factor increase as more stiffening plies are added to

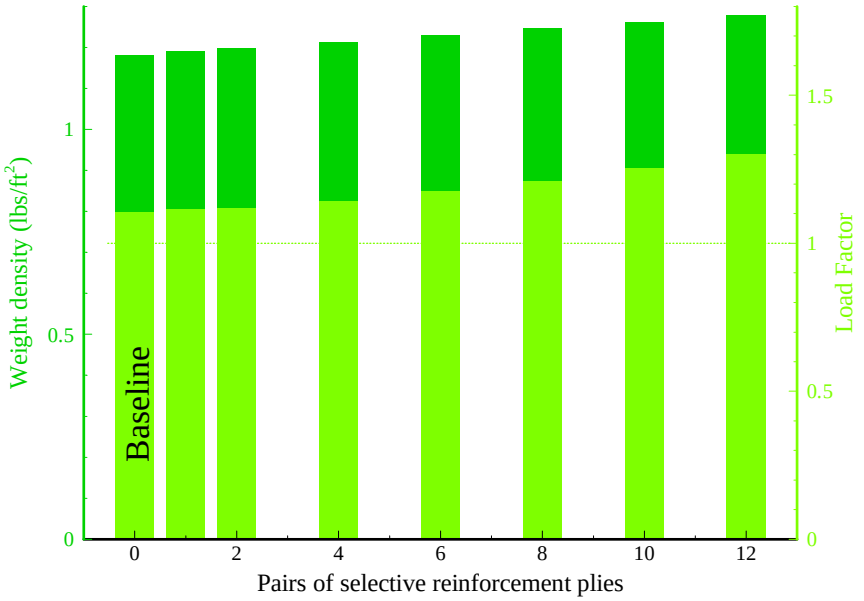

Figure 18: Design Results for Straight Fiber Laminate with Multiple Pairs of Selective Reinforcement Ply Group 4b

the interior of the laminate. Surprisingly, the number of plies within the laminate (ignoring the stiffening plies) is 36 for all designs, even though the load factor approaches a level 30% above the required design load. Above 12 pairs, the selective reinforcement plies constitute 40% of the thickness within the stiffened regions, which would surely degrade the laminate during tow-steering construction.

Similar studies were completed for the best tow-steered construction technique, namely the Overlap method with the vertical stiffness variation. The results were similar as to the straight fiber designs, though at the maximum value of 12 pairs the laminate design did drop down to 28 plies (from 32, the standard solution for this construction technique). However, it is interesting to note that due to the added volume of the internal stiffeners, the actual weight density for the 28-ply tow-steered laminate with 12 pairs of selective reinforcement plies was higher than the best unstiffened tow-steered design (the leftmost data point in Figure 17).

Lastly, several additional design runs were performed stipulating that the stiffening regions were located on the external surface of the laminate. Constructing the laminate in this way produces a much higher risk of a poorly made laminate, since the irregular outer surface may lead to complications during the tow placement process and cure, therefore complete design results were not rigorously sought. For the few runs that were performed, no relative improvement was observed.

4.3 Summary of Results

The results presented in the previous section lead to several points concerning the usefulness of tow-steering and selective reinforcement for the problem under study.

- The monolithic (non-sandwich) designs are not able to compete with the weight density of sandwich panels (from the literature). This is due to the fact that only linear buckling was assessed during the design process (due to limitations of the provided finite element program), which accentuates the usefulness of the sandwich construction technique. Future work should remedy the analysis method or attempt elastic tailoring within the face sheets of a sandwich laminate.

- For the combined loading case presented here, weight improvements using tow-steered plies were only demonstrated by implementing the Overlap method with the variation in the vertical direction. For all other tow-steered construction techniques and directions (Parallel and Tow Drop method in both directions, Overlap method in the horizontal direction), there were only slight, if any, improvements in the buckling load factor as compared to the straight fiber design.

- Inclusion of selective reinforcement plies for the panel with a central hole did not improve the performance of the structure under the given loading conditions. This is generally due to the fact that the stiffening arrangements tended to generate load paths toward the middle of the panel, which in earlier work has been shown to diminish the load carrying capability of a panel under compressive loads. In fairness, the selective reinforcement ply designs were formulated to minimize compliance and did not consider instability of any kind. It is believed that if the load directions were reversed (that is, applying tension as opposed to compression), then the stiffener configurations would alleviate stress concentrations around the central hole and help to reduce the potential of material failure.

References

1. Tatting, B. F., and Gürdal, Z., Design and Manufacture of Elastically Tailored Tow Placed Plates, NASA CR 2002-211919, August 2002.

2. Jegley, D., Tatting, B. F., and Gürdal, Z., "Optimization of Elastically Tailored Tow Placed Plates with Holes," Proceedings of the the 44th AIAA/ASME/ASCE/AHS/ASC Structures, Structural Dynamics and Materials (SDM) Conference, Norfolk VA, April 2003, AIAA Paper No. 1420.

3. Tatting, B. F., and Gürdal, Z., Automated Finite Element Analysis of Elastically Tailored Plates, NASA CR 2003-212679, December 2003.

4. Jegley, D., Tatting, B. F., and Gürdal, Z., "Tow-Steered Panels with Holes Subjected to Compression or Shear Loading," Proceedings of the the 46th AIAA/ASME/ASCE/AHS/ASC Structures, Structural Dynamics and Materials (SDM) Conference, Austin TX, April 2005.

5. Baker, D. J., Ambur, D. R., Fudge, J., and Kassapoglou, C., "Optimal Design and Damage Tolerance Verification of an Isogrid Structure for Helicopter Application," Proceedings of the the 44th AIAA/ASME/ASCE/AHS/ASC Structures, Structural Dynamics and Materials (SDM) Conference, Norfolk VA, April 2003.

6. Setoodeh, S., Gürdal, Z., and Abdalla, M. M., "Simultaneous Topology and Curvilinear Fiber Path Design of Composite Layers using Cellular Automata," Proceedings of the the 45th AIAA/ASME/ASCE/AHS/ASC Structures, Structural Dynamics and Materials (SDM) Conference, Palm Springs CA, April 2004.

7. Setoodeh, S., Gürdal, Z., Abdalla, M. M., and Tatting, B. F. "Design of Variable Stiffness Laminates for In-Plane Loading Using Lamination Parameters," Proceedings of the the 46th AIAA/ASME/ASCE/AHS/ASC Structures, Structural Dynamics and Materials (SDM) Conference, Austin TX, April 2005.

8. Rankin, C. C., Brogan, F. A., Loden, W. A., and Cabiness, H. D., “STAGS Users Manual,” Lockheed Martin Missiles & Space Co., Inc., Report LMSC P032594, June 2000.

Appendix

This appendix is intended to illustrate the steps taken to produce a useful finite element model that (a) incorporates as closely as possible the test conditions of a panel under combined loading; and (b) is small enough to be used for elastic tailoring design techniques. In practice, the goal is to reduce the complexity of the STAGS model supplied by Don Baker of NASA-Langley Research Center to improve the efficiency of the analysis step within the design process. The first part of this document examines the details of the supplied STAGS model (referred to herein as the *test* case), and highlights the relevant portions that need to be correctly modeled. The second section presents differing levels of complexity of simpler models (referred to as *ideal*) that hope to capture the essence of the full solution but which are appreciably smaller in size (with regard to number of nodes, elements, and/or structural components). Once a suitable ideal model is discovered, the third section details the assumptions used to generate a constant grid-size model that can be used within the Cellular Automata design paradigm.

STAGS Finite Element Model

A three-dimensional representation of the finite element model is shown below. The model consists of a test panel (the regular grid in the center region) attached on each side to a picture-frame-type fixture that is

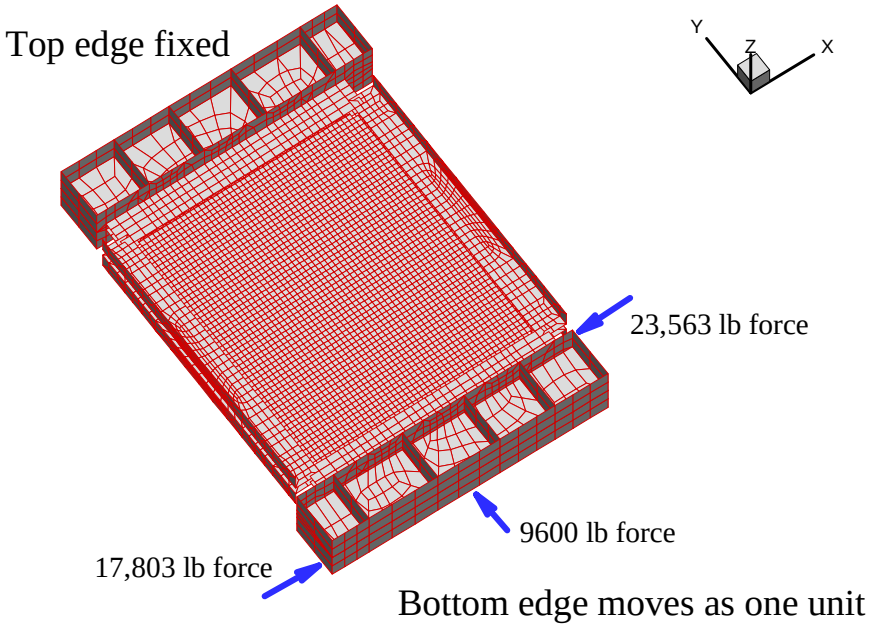

connected by pins, which is attached to appropriate loading frames to achieve the combined loading stress state. During testing, the top edge of the upper frame is held fixed, while the bottom frame undergoes a vertical force from below and a horizontal force through an L-extension of the bottom frame (not shown here). This results in a horizontal force as well as a bending moment, which is represented in the STAGS model by the force couple shown. Relevant details for each component of the testing apparatus follow.

The test panel area is 24 inches wide and 28 inches high, with a grid size of one-half inch in both directions. The original model is assumed to be composed of aluminum (E = 10.0 Msi, ν = 0.33) with a thickness of 0.125 inches. One element is removed at each corner of the test coupon to alleviate stress. Tabs are present on all four sides. The top and bottom tabs measure 23 inches wide (due to the 1/2 cut-out in each corner) by 2.94 inches high, while the sides are 27 inches high and 2.25 inches wide. The tabs are constructed with a layer of steel (E = 30.0 Msi, ν = 0.30, 0.19 inches thick) bonded to each side (though the tab material may change for composite materials, we can assume that one will be present). The test panel and tabs are shown in the figure below with the other components removed. The origin of the axes is in the bottom left corner of the test panel. Note that the meshing within the tabbed regions is quite erratic, which is due to the fact that earlier models possessed higher density meshes within the test panel region along with the fact that certain points within the tab had to be defined as nodes. These nodes are denoted by the colored dots in the figure, and represent the points of attachment between the tabbed

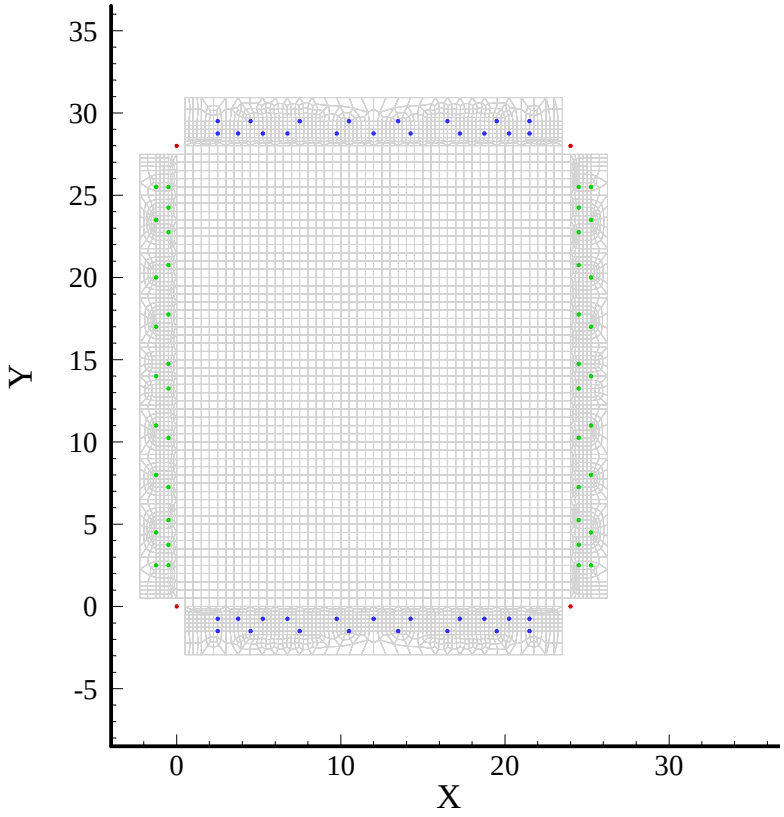

regions and the fixture. The blue dots represent nodes in the tabs which are defined within the model as having identical displacements (horizontal u, vertical v, and out-of-plane w) as the corresponding point in the frame. The green dots are similarly defined, but are only constrained in the u and w displacement directions (the connections in the side fixtures are slotted to allow vertical movement). The red dots shown here represent the pinned connections between horizontal and vertical components of the fixture, and indicate that the displacements for each connected component is identical at that point (note that no connection to the test panel or tabbed areas exist for these red points, but are shown for completeness).

The fixture attached to the test panel is shown in the three-dimensional figure below (only the top fixture is shown, it is symmetric about the *xy*-plane. The test panel is situated below this structural component). The coloring of each element denotes the shell wall property assigned to it within the model definition.

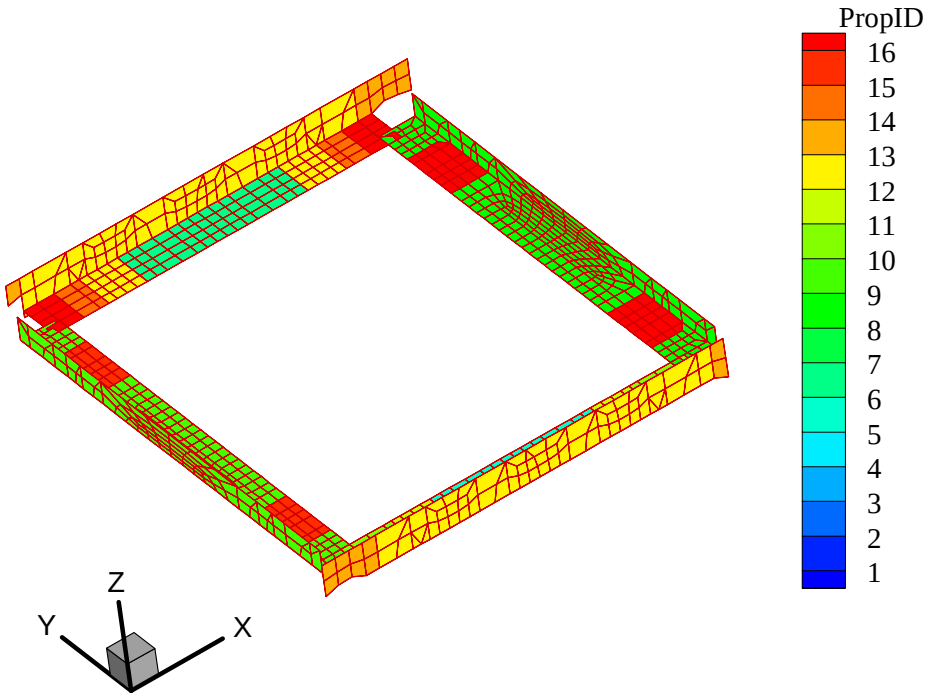

Property IDs 5, 6, 8, and 9 (shades of green), which make up the bulk of the vertical and horizontal frame components within the plane of the test panel, are made of steel with a thickness of 1/2 inches. The red areas within the side frames (IDs 15 and 16) are made of thicker steel (1 inch), as are the yellow regions within the top and bottom frames. Finally, the red areas within the top and bottom frame (the region in the bottom area is hidden, but it is identical to the top frame) have a thickness of 1 1/2 inches, also steel. The frames are connected to each other at the corners (corresponding to the red dots shown in the figure of the test panel) through stipulation that the displacements for the corresponding nodes in each frame are the same. However, for the connection of the bottom frame with the two side frames, the *v*-displacement is again allowed free due to the slotting of the connection point. To summarize, this (upper) frame is made of four steel L-beams, which range in thickness from 1/2 to 1 1/2 inches. A similar lower frame exists, symmetric about the *xy*-plane. Dimensions of the frame are not significant, as long as they are wide enough to cover the tabbed areas (for reference, the top and bottom frames are 3 inches high, while the side frames are 2.25 inches wide). The upper and lower frames are connected to each other by bolts/pins through the tabbed areas that they envelop, and each vertical/horizontal component is also connected to each other through pins at the corners of each frame element. Note that these frames are quite rigid, especially in the areas with the extra thickness.

Lastly, the loading frame shown in the first figure is a steel structure that is loaded by external forces. Note that the loading frame components are not perfectly rigid, but are constructed of thick steel plates that inhibit most of the deformation (relative to the deformation of the test panel). The top of the uppermost loading frame is defined by zero displacements, while the bottom loading frame is constrained by constant *v*-displacement along the lower face and constant *u*-displacement along the right face (as well as zero *w*-displacement everywhere. This effectively limits the rotation of the load frame even when a bending moment is applied to it.

The bottom loading frame is 5.5 inches high. Thus the center of this structural component is 19.75 inches from the center of the test panel where the horizontal shear force is applied [19.75 inches = 28/2 (half the test panel height) + 3 inches (the attachment frame/tabbed area) + 5.5/2 (half the loading frame dimension)]. Thus the bending moment at the center of the load frame for a 5760 lb force applied at the center of the test panel is 113,760 in-lbs, which has been separated into a resultant force-couple and applied at the top and bottom edges of the loading frame.

Buckling Solution (Case:* test*)

For the applied loads, the in-plane and linear buckling solution for the *test* case:

u-displacement of top edge (*x*=12, *y*=28)	=	-0.000247
u-displacement of bottom edge (*x*=12, *y*=0)	=	-0.023611
Relative *u*-displacement	**=**	**-0.023364**
v-displacement of top edge (*x*=12, *y*=28)	=	0.0001084
v-displacement of bottom edge (*x*=12, *y*=0)	=	0.0067016
Relative *v*-displacement	**=**	**0.0065932**
v-displacement of bottom edge node (*x*=21.5, *y*=0)	=	0.0064069
Relative rotation of bottom edge	**=**	**-3.102×10^{-5} radians**
Eigenvalue of linear buckling solution	**=**	**0.73299**

Suitable models should provide reasonable agreement with the quantities in bold, as well as exhibiting similar trends with respect to the stress variation and deformation patterns.

Reduced Models

In an effort to diminish the size of the models, an effort was made to concentrate on the constraints of the test panel component and remove as many other structural components as possible. In general, it was assumed that the relatively rigid steels tended to move as rigid bodies, and by using suitable edge constraints for the test panel an analogous response could be produced. This section, therefore, starts with a model with the broadest assumptions, analyzes it and notes the discrepancies with the test case, and tries to improve the correlation between the two by adding another detail of the complex model. Results and discussion of each successive model follows.

Constant* v*-displacement on bottom edge (Case:* idealV*)

The most basic case modeled only the test panel component, without the tabbed areas but including the notched corners. Identical grid spacing was used (1/2 inch square), and the model was constrained in the following manner: (a) displacement $w = 0$ on all edges, along with rotations about the x– and y-axes, which approximates a clamped condition; (b) u and v displacements are zero along the top edge, which fixes the structure in space; (c) bottom edge has all nodes with identical u and v displacements; (d) side edges have constraint on u-displacement to vary linearly along the edge, from zero at the top to the unknown u-displacement of the bottom edge at the bottom. The loading was applied using a horizontal force of –2760 lbs and a vertical force of 9600 lbs at the center of the bottom edge. A figure showing the mesh with the deformation magnified 200 times is shown on the next page.

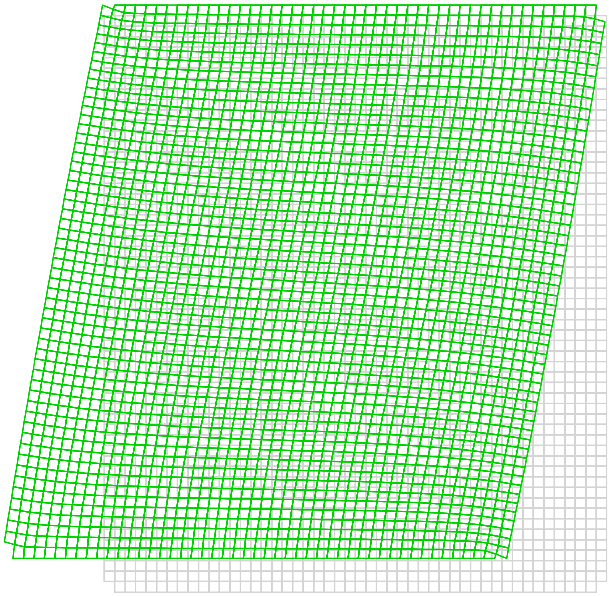

The solution data for this case *idealV*:

u-displacement of top edge (*x*=12, *y*=28)	=	0.0
u-displacement of bottom edge (*x*=12, *y*=0)	=	-0.024306
Relative *u*-displacement	**=**	**-0.024306**
v-displacement of top edge (*x*=12, *y*=28)	=	0.0
v-displacement of bottom edge (*x*=12, *y*=0)	=	0.0080245
Relative *v*-displacement	**=**	**0.0080245**
v-displacement of bottom edge node (*x*=21.5, *y*=0)	=	0.0080245
Relative rotation of bottom edge	**=**	**0.0 radians**
Eigenvalue of linear buckling solution	**=**	**0.49044**

The constraints applied to this structure basically assume infinite stiffness of the loading frame and no allowance for rotation of the bottom edge. Though the *u*-displacement solution is relatively comparable to case *test*, both the *v*-displacement and the eigenvalue indicate that the model is not adequate for our needs. Investigation of the stress variation indicates that the loading here is symmetric about the vertical center of the panel and does not show any skewness with respect to the shear loading, which is evident in the *test* case solution.

Rotation allowed on bottom edge (Case:* idealM*)

To alleviate one of the problems of the earlier model, the constraints along the bottom edge were changed to allow for rotation of the edge. Instead of identical *v*-displacements, vertical motion along the bottom edge was constrained to vary linearly with respect to two unconstrained *v*-displacements: the one at the center and at the rightmost point along the bottom edge. A bending moment was also introduced using a force-couple combination. For the bottom edge, the resultant moment for a horizontal force applied at the center of the panel is calculated as [5760 lbs × 14 inches = 80,640 in-lbs], which is broken into a vertical downward force of 7012 lbs applied at the center of the bottom edge and an upward force at the rightmost edge, 11.5 inches away [80,640/11.5 = 7012]. At the center of the bottom edge, a vertical force of 9600

lbs is already being applied, so the resultant force applied there is 2588 lbs. The rest of the constraints are identical to the ones applied for the previous case.

The solution data for this case *idealM*:

u-displacement of top edge (*x*=12, *y*=28)	=	0.0
u-displacement of bottom edge (*x*=12, *y*=0)	=	-0.024306
Relative *u*-displacement	**=**	**-0.024306**
v-displacement of top edge (*x*=12, *y*=28)	=	0.0
v-displacement of bottom edge (*x*=12, *y*=0)	=	0.0080245
Relative *v*-displacement	**=**	**0.0080245**
v-displacement of bottom edge node (*x*=21.5, *y*=0)	=	0.0080242
Relative rotation of bottom edge	**=**	**-3.158×10^{-8} radians**

Eigenvalue of linear buckling solution = 0.49044

In summary, hardly any change from the previous case. The rotation was small enough to be almost indiscernible and had no apparent affect on the buckling load. The large discrepancy in the *v*-displacement was still a major concern, and indicated that the *test* case possessed more stiffness than the idealized model that was being used.

Inclusion of tabbed regions (Case:* idealT*)

To improve the stiffness of the model, the tabbed regions were added to the model with no other changes to the previous constraints (from case *idealM*). It was reasoned that since the *v*-displacement along the vertical edges was unconstrained, the material within the tabbed regions played a major role in the stiffness of the panel. Therefore, elements were added to the model that corresponded exactly to the dimensions and shell wall construction of the *test* case model. That is, the top and bottom tabs were 2.94 inches high and constructed of a 0.125 inch aluminum layer sandwiched by two steel layers of 0.19 inches, while the side tabs were 2.25 inches wide and constructed with the same layup. It should also be noted that each tab region used four elements across it, which were not necessarily regularly spaced. The top/bottom were spaced with intervals {0.75, 1.5, 2.25, 2.94} inches with regular spacing in the horizontal direction, while the elements within the side tabs were located at {0.5, 1.25, 1.75, 2.25} and regular spacing in the vertical direction. These choices were made to conform to the correct dimensions and to serve as useful points for the connection point constraints further down the evolution of the model (discussed in detail later).

For the new nodes within the tabbed regions, the only applied constraint was to enforce zero *w*-displacement for all points. Because of the presence of this constraint and the added material within the tab shell walls, the constraints on the rotations about the *x* and *y* axes that were stipulated for all edges (in case *idealV*) were removed.

The solution data for this case *idealT*:

u-displacement of top edge (*x*=12, *y*=28)	=	0.0
u-displacement of bottom edge (*x*=12, *y*=0)	=	-0.021781
Relative *u*-displacement	**=**	**-0.021781**
v-displacement of top edge (*x*=12, *y*=28)	=	0.0
v-displacement of bottom edge (*x*=12, *y*=0)	=	0.0055136

Relative *v*-displacement	**=**	**0.0055136**
v-displacement of bottom edge node (*x*=21.5, *y*=0)	=	0.0055136
Relative rotation of bottom edge	**=**	**0.0 radians**
Eigenvalue of linear buckling solution	**=**	**0.67506**

As expected, the presence of the tabs increased the stiffness, thereby increasing the buckling load value and decreasing the vertical displacement of the bottom edge. It also decreased the rotation of the bottom edge to insignificant magnitude. However, the presence of the tabbed regions also introduced some skewness to the shear stress resultant, which followed the basic trend of the *test* case solution. Therefore it was believed that the inclusion of the more accurate edge conditions was a significant improvement. A check was also needed on the edge rotation, since some rotation of the lower edge was expected.

Transformation to edge rotation constraint (Case:* idealW*)

To check the validity of the straight edge constraints, a different approach was used to model the rotation of the bottom edge. Note that in case *idealM*, the linear variation of the bottom edge was constrained in terms of two vertical displacements, one in the center and one at the edge. To verify that this method was introduced the constraint and the loading as expected, the straight edge constraint was altered so that the displacement of each point along the bottom edge was dependent on the relative translation and rotation of the point at the center of the bottom edge. Thus, the *u*-displacement constraint stayed the same, while the *v*-displacement constraint became:

$$v(x) = v_0 + [x]\omega_0 \tag{2}$$

where the zero subscript denotes the point at the middle of the bottom edge. Besides this new constraint, the loading was changed by introducing a corresponding moment about the middle edge point. Thus the loading consisted of a vertical force of 9600 lbs, a horizontal force of –5760 lbs, and a bending moment about the *z*-axis of 80,640 in-lbs.

The solution data for this case *idealW*:

u-displacement of top edge (*x*=12, *y*=28)	=	0.0
u-displacement of bottom edge (*x*=12, *y*=0)	=	-0.021781
Relative *u*-displacement	**=**	**-0.021781**
v-displacement of top edge (*x*=12, *y*=28)	=	0.0
v-displacement of bottom edge (*x*=12, *y*=0)	=	0.0055136
Relative *v*-displacement	**=**	**0.0055136**
v-displacement of bottom edge node (*x*=21.5, *y*=0)	=	0.0055137
Relative rotation of bottom edge	**=**	**-1.044×10^{-8} radians**
Eigenvalue of linear buckling solution	**=**	**0.67506**

These results indicate that either method of constraint/loading works equally well (displacement constraints with pure force loading versus rotation constraint with force/moment loading), which bodes well for future solutions.

Turning our attention back to the results with regard to the deformation of the *test* case, both the translation displacements of the bottom edge are smaller than the expected value. This implies that the stiffness of our ideal model still does not match up exactly with the more complex model. Thus it was reasoned that a more accurate modeling of the load introduction through the top and bottom tabs is required, since the constraints presently applied to the edges of the test panel region seem quite prohibitive. Additionally, examination of the vertical displacements along the entire bottom edge for cases *test* and *idealW* reveal a startling disparity, as shown in the figure below:
Besides the disparity of magnitude, the graph reveals that the straight edge constraint assumed at the

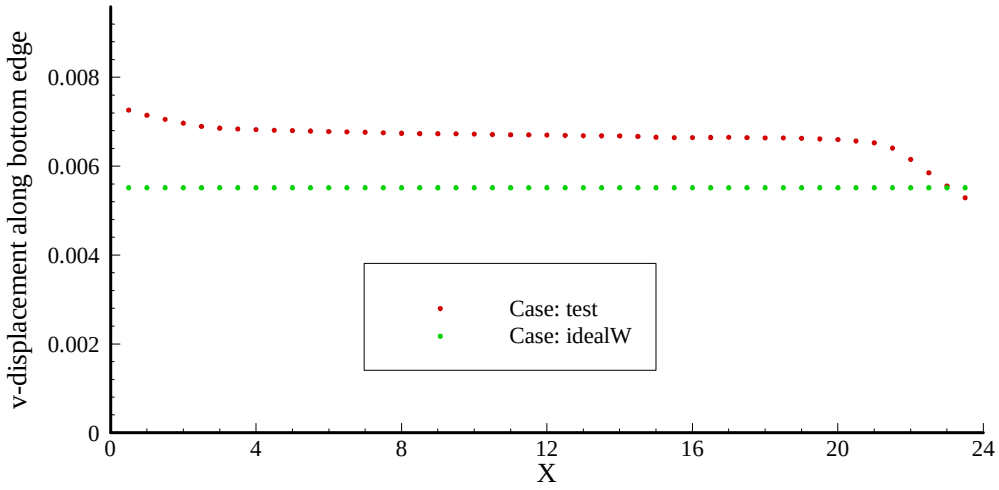

edges does not hold true for the *test* case near the extremities of the edges. This is due to the fact that the connection points to the test panel (shown by the colored dots in the figure on page 2) do not extend to the ends of the edges, but stop 2.5 inches short of it for each fixture. This results in the sharp variation of the displacements as shown above, and will also greatly affect the stiffness response of the panel.

Load application through fixture connections (Case:* idealF*)

To account for the non-uniform loading through the connection points within the tabbed regions, a more complex constraint system was introduced. The system is based on the assumption that the connection points move as a rigid body within each frame member. The reference point for the translation and rotation of the bottom edge is shifted to the middle point within the tabbed area, and the loading is applied there as well (note that due to the new location, the applied moment is now 84,960 in-lbs). The following figure and associated equations describe the method of constraint, where the color coding of the remarks and equations correspond to the colored dots in the figure.

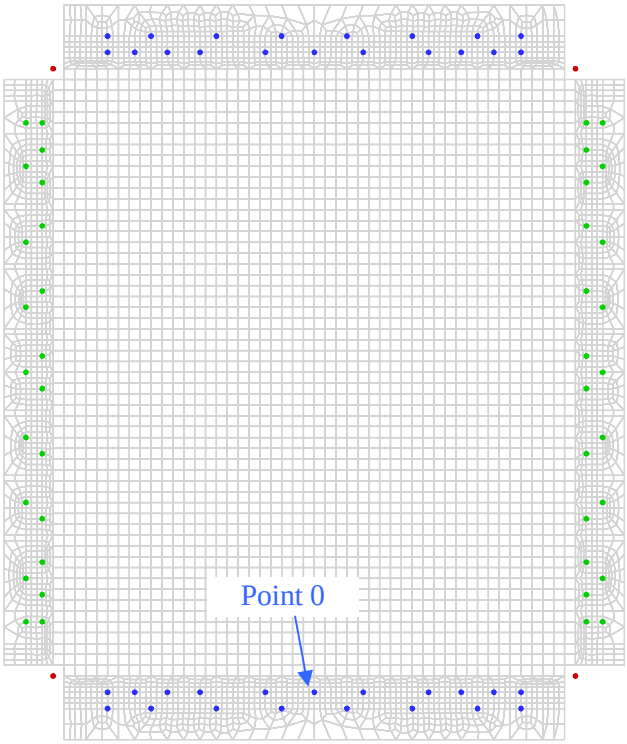

All points within tabbed areas:

$$w = 0 \tag{3}$$

Points within top frame:

$$u = v = 0 \tag{4}$$

Frame connection points at top:

$$u = v = 0 \tag{5}$$

Points within bottom frame:

$$u = u_0 - [x - x_0]\omega_0 \qquad v = v_0 + [y - y_0]\omega_0 \tag{6}$$

Frame connection points (hinges) at bottom:

$$u_{hinge} = u_0 - [0.75]\omega_0 \qquad v_{hinge} = \text{unconstrained} \tag{7}$$

Points within vertical frame members:

$$u = -[y - y_{hinge}]\frac{u_{hinge}}{28} \tag{8}$$

To summarize, the connection points within the top tabbed region are set to be zero. This assumes a rigid frame that is not allowed to move. Since the top connection points are within the top frame, they too are constrained to be zero. For the bottom frame, the horizontal and vertical displacements are assumed move as a rigid body about Point 0, where the rotation is now also included in the *u*-displacement constraint. Calculations for the connection points (referred to as hinges for they are the pinned hinge between the bottom and the side frames) are calculated in Eq. (7), though it should be remembered that the *test* case model does not enforce any constraint in the vertical direction for this hinge. Since the *u*-displacement for

the top and bottom hinges are now both known (or expressed in terms of the displacements at Point 0), the linear equation for the *u*-displacements within the side frames follows.

The solution data for this case *idealF*:

u-displacement of top edge (*x*=12, *y*=28)	=	-0.000006
u-displacement of bottom edge (*x*=12, *y*=0)	=	-0.022912
Relative *u*-displacement	**=**	**-0.022908**
v-displacement of top edge (*x*=12, *y*=28)	=	0.0000250
v-displacement of bottom edge (*x*=12, *y*=0)	=	0.0057571
Relative *v*-displacement	**=**	**0.0057321**
v-displacement of bottom edge node (*x*=21.5, *y*=0)	=	0.0055994
Relative rotation of bottom edge	**=**	**-1.660×10^{-5} radians**
Eigenvalue of linear buckling solution	**=**	**0.65810**

Unfortunately, application through the connection points seemed to make the agreement worse, at least on the surface. However, comparison of the results between this case and the *test* case revealed that though the magnitudes of the numbers were not comparable (especially the buckling eigenvalues), the variations of the field quantities were following the same basic trends. Therefore, only a few more adjustments were required. To gain insight into the motivation behind the last improvement, plots of the N_x stress resultant are shown for the test panel and tabbed regions for both the *test* case and *idealF*. The color of each element represents the level of magnitude of the stress resultant.

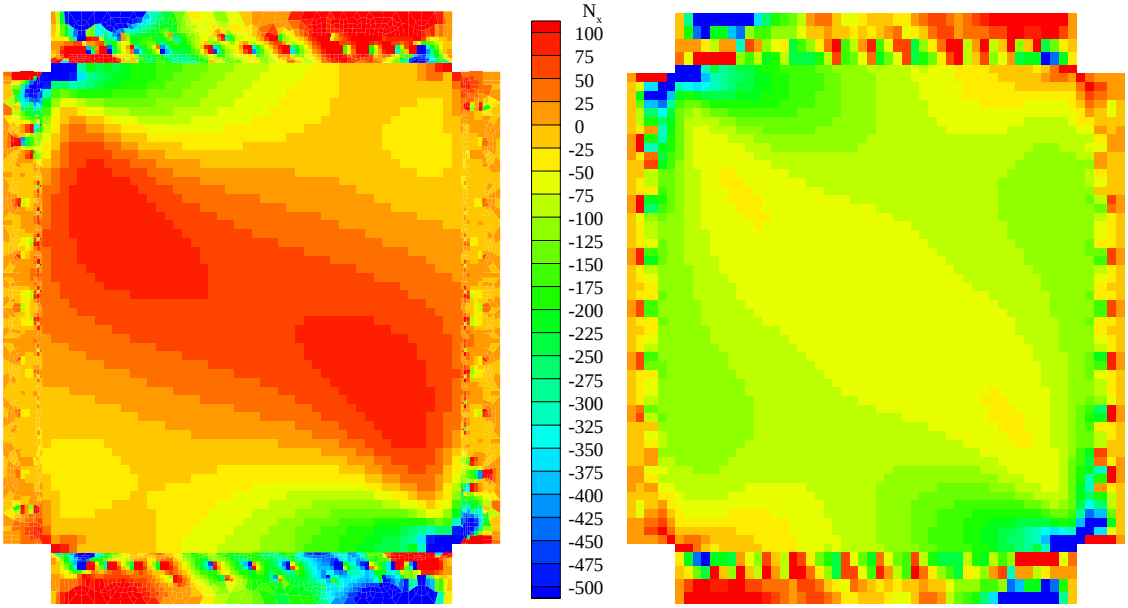

Case: test Case: idealF

The surprising result indicated by these results is that the *test* case actually exhibits a positive value of the N_x stress resultant in center of the panel. Except for this discrepancy, the other resultants for the two cases look reasonably similar, yet the disparity highlighted here would lead directly to the differences in eigenvalues for the two cases. Therefore, more attention was focused on the side edges of the panel. The *ideal* cases have been assuming straight edges along the length, but closer inspection revealed that the *test*

case did not follow this rule and exhibited some deformation along the length of the vertical tabbed regions.

A plot of the *u*-displacement as a function of *y* for the right edge of the connection line (a vertical line within the right-side tabbed regions that would go through the green points closest to the center of the panel) is shown on the next page for both cases. As one would expect, the linear constraint applied to the connection points for the *idealF* case maintains a relatively straight line during deformation (some slight nonlinearity is present near the ends, outside of the connection point region). However, the *test* case reveals that significant nonlinearity is present in the middle of the region as well. In physical terms, the vertical compressive load applied to the test panel introduces expansion in the horizontal direction due to the Poisson effect. However, the side frames resist this expansion. For the *idealF* case, the side frames (and therefore the connection points within the tabbed area) are assumed to be rigid with respect to horizontal deformation, therefore this results in a compressive N_x stress resultant as evidenced by the N_x plots shown above (the plot on the right). In actuality, the side frames are not rigid but experience elastic deformation due to the expansion of the test panel. This allows for more expansion of the test panel and results in a tensile field in the horizontal direction for the *test* case (see the plot on the left in the figure above). Therefore, for our ideal models to match the test conditions, some relaxation of the rigid side constraints are required.

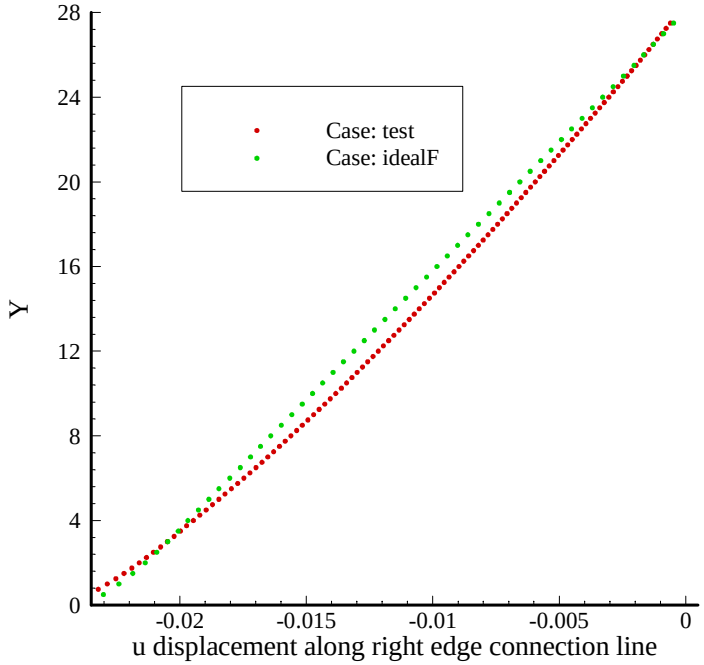

At this point, a choice had to be made. To most correctly model the elasticity of the vertical tabbed regions, attachments to the framing components (shown in the figure on page 3) should be modeled by constraining them to move with the nodes of the frames, which would have to be added to the model. This would closely follow the technique employed for the *test* case model, but would involve added many nodes and elements (which would reduce the all-important analysis time). Alternatively, the present *idealF* model could be slightly altered to allow for some relaxation of the vertical tabbed regions.

Relaxation of linear constraints within side tabs (Case:* idealR*)

Closer examination of the *test* case deformation revealed that though the displacements along the edge looked nonlinear, the points within the thicker steel regions of the frame (as indicated by the red areas for the right frame in the figure on page 3) followed a linear variation more closely than the rest of the frame. Therefore, an *ad hoc* relaxation of the linear constraint could be accomplished by removing the constraints for the connection points outside of the thicker region of the frame. Note that this assumption is not exact, since the movement of these points do possess a correspondence to the deformation of the frame. Nevertheless, the constraints for the *u*-displacement for the vertical tabs were limited to the top and bottom five points on each side, corresponding to the thicker region of steel for the frame (which is 1 inch thick as opposed to 1/2 inch thick for the rest of the frame).

The solution data for this case *idealR*:

u-displacement of top edge (*x*=12, *y*=28)	=	-0.000055
u-displacement of bottom edge (*x*=12, *y*=0)	=	-0.022918
Relative *u*-displacement	**=**	**-0.022863**
v-displacement of top edge (*x*=12, *y*=28)	=	0.0000238
v-displacement of bottom edge (*x*=12, *y*=0)	=	0.0060548
Relative *v*-displacement	**=**	**0.0060310**
v-displacement of bottom edge node (*x*=21.5, *y*=0)	=	0.0058934
Relative rotation of bottom edge	**=**	**-1.700×10^{-5} radians**
Eigenvalue of linear buckling solution	**=**	**0.72216**

The resulting displacements along the vertical connection line are shown below:. As expected, the

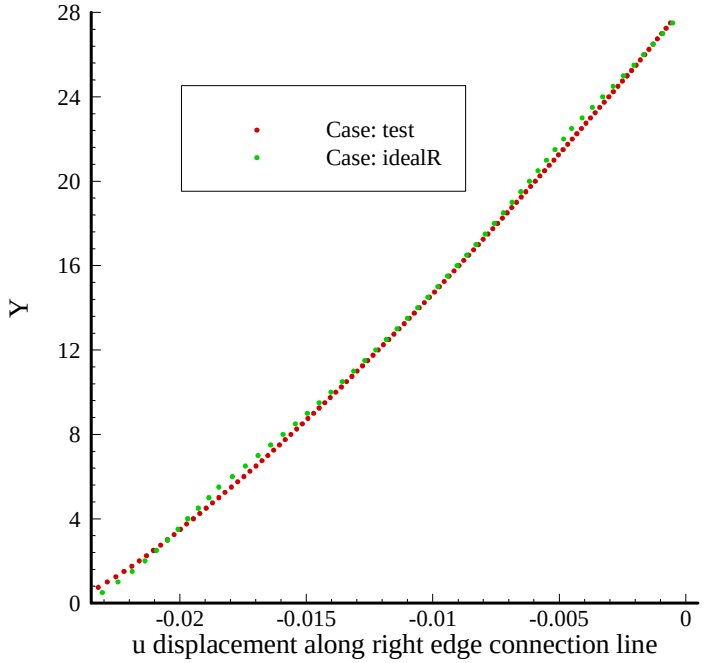

relaxation of the rigid frame results in much better agreement between the two cases, though the regions within the constrained thick frame region are still imperfectly modeled. However, the excellent agreement between the *idealR* case and the *test* model for the displacements and eigenvalue estimate indicate that this case is adequate for design purposes.

Model Definition for Cellular Automata Design (Case: idealCA)

Lastly, some slight modifications to the best ideal model are required for easy implementation of the Cellular Automata design paradigm. The two major modifications include: (a) regular grid spacing of all elements; and (b) enforcement of constraints through displacements only.

The first of these modifications is satisfied by changes the dimensions of the elements within the tabbed regions of the model. For the top/bottom region, the vertical spacing of the elements is altered from four elements aligned at {0.75, 1.5, 2.25, 2.94} inches to six elements located at {0. 5, 1.0, 1.5, 2.0, 2.5, 3.0}, which satisfies the 1/2 grid size of the model. Along with the location change, the connection points are moved from their previous location of 0.75 and 1.5 to 1.0 and 1.5. Along the length of the horizontal tabs, the points are located at {2.5, 4, 5.5, 7, 10, 12, 14, 17, 18.5, 20, 21.5} for the line closest to the panel center and {2.5, 4.5, 7.5, 10.5, 13.5, 16.5, 19.5, 21.5} for the exterior line. For the vertical tabs, the spacing changes from {0.5, 1.25, 1.75, 2.25} to {0.5, 1, 1.5, 2}, resulting in a smaller tab size on the sides. The locations of the points within the thick region of the frame are {2.5, 4, 5.5, 22.5, 24, 25.5} for the line closest to the panel center and {2.5, 4.5, 23.5, 25.5} for the outside line.

Changing the straight edge constraints back to displacement equations results in the following alterations to the constraint equations:

Points within bottom frame:

$$u = u_0 \qquad v = v_0 + [x - x_o]\frac{(v_{x=21.5} - v_0)}{9.5} \tag{9}$$

Points within vertical frame members:

$$u = -[y - y_{hinge}]\frac{u_0}{28} \tag{10}$$

Implementation of these changes leads to the following results for case *idealCA*:

u-displacement of top edge (*x*=12, *y*=28)	=	-0.000072
u-displacement of bottom edge (*x*=12, *y*=0)	=	-0.022836
Relative *u*-displacement	**=**	**-0.022764**
v-displacement of top edge (*x*=12, *y*=28)	=	0.0000302
v-displacement of bottom edge (*x*=12, *y*=0)	=	0.0061293
Relative *v*-displacement	**=**	**0.0060991**
v-displacement of bottom edge node (*x*=21.5, *y*=0)	=	0.0060623
Relative rotation of bottom edge	**=**	**-7.053×10^{-6} radians**
Eigenvalue of linear buckling solution	**=**	**0.71818**

The deformed shape for the two cases are shown on the next page, magnified 200 times.

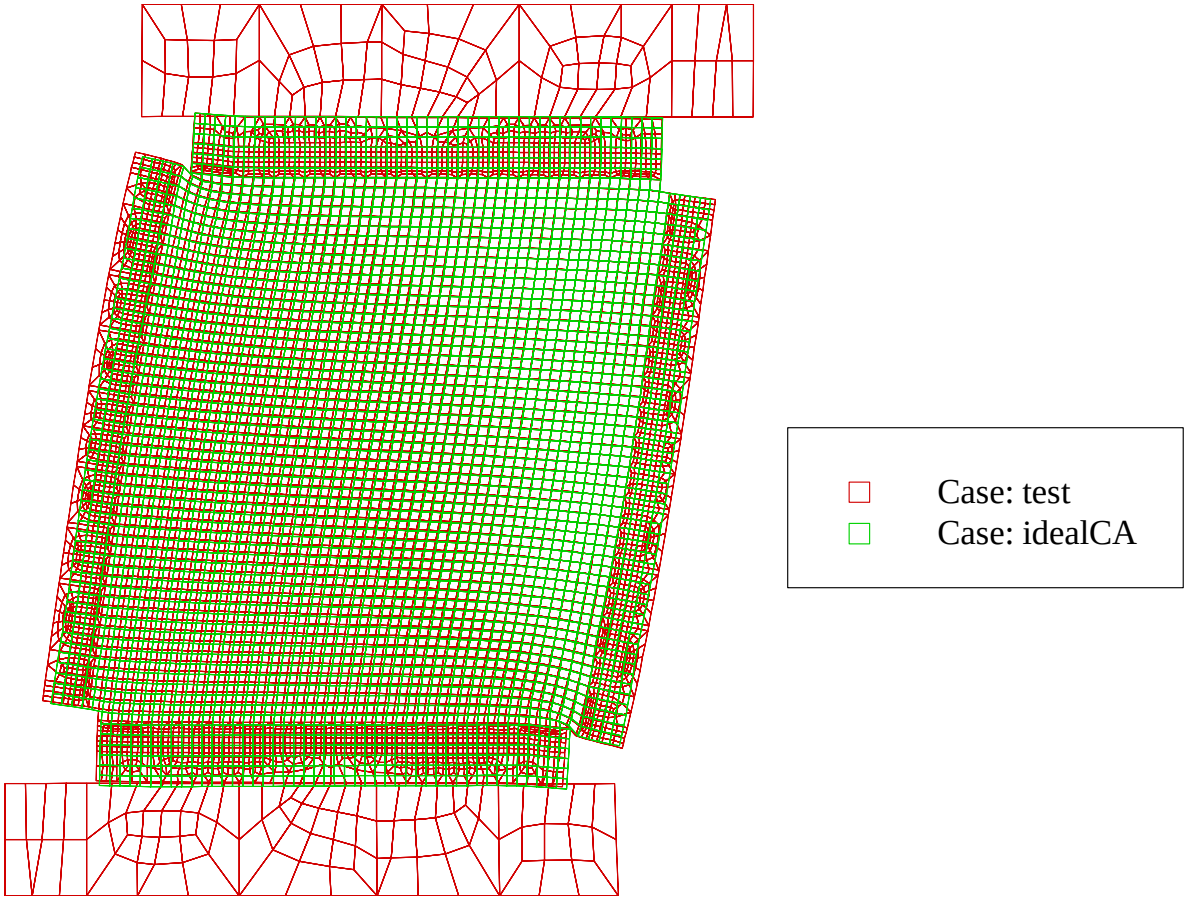
Case: test
Case: idealCA

REPORT DOCUMENTATION PAGE

Form Approved
OMB No. 0704-0188

1. REPORT DATE *(DD-MM-YYYY)*	2. REPORT TYPE	3. DATES COVERED *(From - To)*
01- 09 - 2005	Contractor Report	

4. TITLE AND SUBTITLE

Enhancements of Tow-Steering Design Techniques: Design of Rectangular Panel Under Combined Loads

5a. CONTRACT NUMBER

NAS1-00135

5b. GRANT NUMBER

5c. PROGRAM ELEMENT NUMBER

6. AUTHOR(S)

Tatting, Brian F.; Setoodeh, Shahriar; and Gürdal, Zafer

5d. PROJECT NUMBER

5e. TASK NUMBER

5f. WORK UNIT NUMBER

23-064-30-34

7. PERFORMING ORGANIZATION NAME(S) AND ADDRESS(ES)

NASA Langley Research Center
Hampton, VA 23681-2199

8. PERFORMING ORGANIZATION REPORT NUMBER

9. SPONSORING/MONITORING AGENCY NAME(S) AND ADDRESS(ES)

National Aeronautics and Space Administration
Washington, DC 20546-0001

10. SPONSOR/MONITOR'S ACRONYM(S)

NASA

11. SPONSOR/MONITOR'S REPORT NUMBER(S)

NASA/CR-2005-213911

12. DISTRIBUTION/AVAILABILITY STATEMENT

Unclassified - Unlimited
Subject Category 39
Availability: NASA CASI (301) 621-0390

13. SUPPLEMENTARY NOTES

Zafer Gürdal: Departments of Engineering Science and Mechanics, and Aerospace and Ocean Engineering, Virginia Polytechnic Institute and State University, Blacksburg, Virginia, currently, Chair, Delft University of Technology, 2629 HS Delft, The Netherlands. Technical Monitor: Dawn C. Jegley. An electronic version can be found at http://ntrs.nasa.gov

14. ABSTRACT

An extension to existing design tools that utilize tow-steering is used to investigate the use of elastic tailoring for a flat panel with a central hole under combined loads of compression and shear. The tailoring is characterized by tow-steering within individual lamina and Cellular Automata design concepts based on selective reinforcement. Designs using traditional straight fiber plies, and tow-steered designs using parallel, tow-drop, and overlap plies within the laminate were generated. These results indicated that the overlap produces the method most structurally efficient designs compared to traditional constant stiffness monocoque panels, though the laminates were not as efficient as sandwich and isogrid designs. Further design studies were conducted using selective reinforcement plies at the core and outer surface of the laminate, however, the minimization of the compliance directs the major stresses toward the center of the panel, which decreased the ability of the structure to withstand loads leading to instability.

15. SUBJECT TERMS

Tow-steering; Curvilinear fibers; Composite structures; Selective reinforcement; Optimization; Combined loading; Graphite-epoxy

16. SECURITY CLASSIFICATION OF:			17. LIMITATION OF ABSTRACT	18. NUMBER OF PAGES	19a. NAME OF RESPONSIBLE PERSON
a. REPORT	b. ABSTRACT	c. THIS PAGE			STI Help Desk (email: help@sti.nasa.gov)
					19b. TELEPHONE NUMBER *(Include area code)*
U	U	U	UU	39	(301) 621-0390